2.3 Experimental Study of Thermocapillary Flow in The Half-Zone Liquid Bridge of Low Prandtl Number Fluid

NASDA Space Utilization Research Center

EXPERIMENTAL STUDY OF THERMOCAPILLARY FLOW IN THE HALF-ZONE LIQUID BRIDGE OF LOW PRANDTL NUMBER FLUID

Masahiko Ohtaka [1], Katsuhiko Takagi [1], Hidesada Natsui [2], Tatsuya Arai [1], and Shinichi Yoda [1]

[1] National Space Development Agency of Japan, Sengen 2-1-1, Tsukuba-city, Ibaraki 305-8505, Japan

[2] Advanced Engineering Services Co. Ltd., Takezono 1-6-1, Tsukuba-city, Ibaraki 305-0032, Japan

The first and clear experimental evidence for the transition from the steady to the oscillatory flow was presented by the non-contact temperature measurement of a molten tin surface and the surface flow visualization. Imaishi *et al* comformed validity of the experimentally determined Ma_{c2} and frequency of the standing wave in comparison with a numerical result. Some performance tests for radiation thermometer also made this experimental result reliable and accurate. The effect of an aspect ratio (As) on the Ma_{c2} has been studied. The Ma_{c2} increases with decreasing of As in the range of As□1.24. Internal temperature field of liquid bridge at oscillatory flow was speculated by the phase relation analysis of the simultaneous multi-measurement data of surface temperature. The numerical simulation was conducted under the same conditions of the experiment in order to check the onset point and temperature fluctuation data obtained by the experiment.

The surface tension of molten tin was measured at various temperatures between 523 and 1023K under the oxygen partial pressures (P_{O2}) between 10^{-19} and 10^{-6}MPa. It was clarified an appropriate value of the surface tension coefficient for experimental chamber is -0.9×10^{-4}N/mK. It was also found that the temperature coefficient of surface tension at a constant P_{O2} raised as P_{O2} increased, and the sign of the coefficient changed from minus to plus at log P_{O2}= –9.375MPa.

Visualization technique (3D-UV) of flow field measurements for liquid metals using ultrasonic transducer with high heat resistance has been successively developed for the experiments. Sensitivity of transducer was examined at high temperature condition same as actual thermocapillary experiment. High spatial resolution in the direction of ultrasonic propagation. was obtained. Visualization performance of ongoing sensor-design was confirmed by numerical simulation. The tracer is also currently under development. Technique for improvement of sphericity and surface roughness was developed. Endurance against molten tin and acoustic characteristics of trial production were experimentally examined.

1. INTRODUCTION

It is well known that thermocapillary flow has an undesirable effect on the crystal growth of semi-conductors by the floating zone methods, which lead to striations of the dopant in the crystal. The previous studies, in which a half zone liquid bridge have been often used as a model configuration of the floating zone, have shown that flow and temperature fields were governed by dimensionless parameter of Marangoni (Ma) or Reynolds (Re) number defined as follows:

$$Ma = \frac{|\sigma_T|\Delta TL}{\mu\alpha} \quad (1\text{-}1),$$

$$Re = Ma/Pr \quad (1\text{-}2),$$

σ_T is a temperature gradient of surface tension, ΔT is a temperature difference between hot and cold disks, L is a characteristic length of the fluid, μ is dynamic viscosity, α is thermal diffusivity, and Pr is Prandtl number of the fluid. In this study, a radius (a) of the liquid bridge is used as a characteristic length.

In higher Pr number fluids, it was experimentally proved that a transition from axisymmetric steady to 3D oscillatory flow occurs at a critical Marangoni number (Ma_c). On the other hand, it was numerically predicted that thermocapillary flow in a low Pr number had two transition points [1], [2]: That is, transition from axisymmetric to 3D steady will occur at a first bifurcation point (Ma_{c1}), and transition from 3D steady to oscillatory at a second one (Ma_{c2}). The prediction needs to be experimentally proved.

A detail experiment around the bifurcation point, in which even the Ma_{c2} is predicted to be in the order of 10^1 for a Pr=0.01 liquid bridge [3], is required to prove the transition behavior of Marangoni convection. However, many studies have been conducted at a Marangoni number that is far from the Ma_{c2} because those have mainly focused on a contribution to produce a high quality single crystal from a molten metal.

Nakamura et al. [4], [5] measured a surface temperature fluctuation with a thermocouple in a molten silicon column of 10mm in diameter and 10mm in length, and found that a frequency of the fluctuation was 0.1Hz at a temperature difference of 100K. However, the imposed temperature difference was far from the second bifurcation point. Han et al. [6] experimentally investigated thermocapillary convection in a liquid bridge of mercury. Free surface fluctuations were measured by a non-contacted diagnostic system, and they found the Ma_{c2}, detecting it to be 900 with a frequency around 5Hz. Quite recently, Yang and Kou [7] reported the onset point of temperature fluctuation and its frequency (Ma_{c2}=194 and 1.1Hz) of a molten tin column by the contacted diagnostic, *i.e.* J-type thermocouple. However, disturbances on the flow and temperature field are caused by a thermocouple which contacts with a fluid and a thermocouple often acts as a cold spot which makes it a complicated temperature gradient along a free surface. It should be noted here that there is no successful experiment to verify the transition behavior of thermocapillary flow by a non-contact diagnostic even nearby the Ma_{c2}.

The goal of present study is to understand the transition phenomena of thermocapillary flow by means of an experimental approach and comparative study with the numerical works in this research group.

The experimental efforts began to select a fluid material for a low Pr number liquid bridge in 1998 [8]. The selected material was molten tin of which Pr number is identical

with that of molten silicon (Pr=0.01). Therefore, we can directly compare our experimental result with available experimental and numerical results of molten silicon because the identical Pr number means to show the same fluid dynamic behavior. Moreover, molten tin as a test fluid has an experimental advantage in a detection of Ma_{c2} compared to molten silicon. Since the melting point of tin is much lower than that of silicon, there is no need to use an infrared image furnace for melting a tin sample, which was used for a molten silicon experiment [4] and [5], and an electric heater is applicable to melt it. Thus, it is expected that the surface temperature of a molten tin column can be measured by a non-contact diagnostic with relatively low noise level. The high purity iron was selected as solid material to sustain a liquid bridge because of the reason that moderate wettability and low reactivity against molten tin is required for the solid material[8].

On the other hand, the selected test fluid has a thermodynamic disadvantage which the oxygen partial pressure is extremely low at the equilibrium between molten tin and tin oxides (SnO and SnO_2) near the temperatures for the low Pr experiment (about 570-770K), resulting in suppressing the thermocapillary flow by the formation of an oxide film over a surface of the melt. However, in 1999, we have successfully overcome the difficult problem of oxidation over the tin surface [9]. Consideration concerning the surface science of tin led us to design of a unique experiment apparatus where a clean surface of molten tin can be obtained by the Ar^+ ion etching method and sustained under the high vacuum condition (about 10^{-6}Pa) during an experiment. The performances of the experiment apparatus were already confirmed. In 1999, a non-contact measurement technique of the surface temperature has been also developed to detect small amplitude of temperature fluctuation at around the Ma_{c2} [9]. It was also confirmed that the radiation thermometer which is equipped with the PbS photo detector and combined with the attachments to obtain a high signal-to-noise ratio such as CaF_2 optical pass filter and an isotropic graphite panel had the sufficient temperature resolution to detect the Ma_{c2} with high accuracy. It was concluded that those unique considerations and devices undoubtedly lead us to a success of detecting the transition to oscillatory flow of the low Pr fluid without any flow disturbances.

Compared with the conventional transparent fluid used for a high Pr number experiment, a low Pr number fluid has another experimental difficulty: It is impossible to observe an internal flow field for opaqueness of a low Pr fluid. In order to overcome this problem, a novel visualization technique using an ultrasonic transducer with a high heat resistance has been experimentally studied for an internal flow field measurement since 1999 [9]. The visualization technique also requires a development of a unique balloon-like tracer. A critical condition on the Ma_{c1} and a detail structure of oscillatory flow will be clarified by this measurement technique.

The experimental results with molten tin obtained in 2000 are significant for the thermocapillary convection of a low Pr fluid. As predicted in the last issue [9], we have succeeded in detection of the transition to oscillatory flow by the surface temperature measurement without any flow disturbances. The flow transition was verified by comparison of the experimentally obtained Ma_{c2} and frequency of surface temperature fluctuation with the numerical results, and by a surface flow visualization experiment directly [10]. The effect of the liquid bridge geometry on the Ma_{c2} and oscillation frequency was further investigated and discussed [11]. The following results are described in this study:

(1) Experimental verification of surface temperature measurement (in-house activity)
(2) Detection of transition phenomena to oscillatory flow (in-house activity)
(3) Effect of aspect ratio on the critical condition and flow structure (in-house activity)

(4) Numerical simulation for the specific case (in-house activity, collaboration with Kyushu University)
(5) Oxygen partial pressure dependence of surface tension of molten tin (collaboration with Kyushu Institute of Technology)
(6) Development of measuring technique of internal flow field (entrusted to Toshiba Co. and, partly, Sukegawa Electric Co. Ltd.)
(7) Development of visualization tracer (collaboration with Kagoshima Prefectural Institute of Industrial Technology and partly entrusted to NTT Advanced Technology Co.)

2. OSCILLATORY THERMOCAPILLARY FLOW OF MOLTEN TIN

2.1 Experimental Verification of Surface Temperature Measurement Technique

In 1999, resolution of radiation thermometer under same experimental conditions was experimentally verified according to Japan Industrial Standard (JIS)[9].

In present work, other performances were verified by simple experiment using available instrument to make the data taken by thermocapillary experiment more accurate and reliable.

2.1.1 Size of Measuring Area

A size of measuring area was experimentally measured by optical pinhole scan. Figure 2-1 shows the experimental setup. The optical pinhole (Diameter: 500ìm) was used to measure a size of measuring area. The constant radiation energy of tungsten halogen lamp was used as measuring object. The pinhole was moved by micro positioning stage at 100ìm step. The result is shown in Fig. 2-2. The signal level is almost equal with segment of 1mm in length. At both sectional ends of 2mm in length, the signal level is sharply attenuated into approximately 65% of maximum level. It was confirmed that the size of measuring area, in which equal signal level is outputted by receiving constant radiation energy, is about 1mm in diameter.

2.1.2 Frequency Characteristics

A nominal value of response time shown in manufacturer's operation manual is 2msec (500Hz). This capability is fast enough for thermocapillary experiment. The frequency response characteristic in the region lower than 10Hz, which is substantial frequency range to detect the temperature fluctuation of oscillatory flow, was measured in detail. Figure 2-3 shows the experimental setup. A measuring object was tungsten halogen lamp whose lighting intensity was held at same radiation level as molten tin of thermocapillary experiment. A light chopper was used and set between light source and the radiation thermometer in order to simulate the temperature change at constant frequency. The time series data of 9 kinds of frequencies (1Hz - 9Hz at 1Hz intervals) were recorded at 20Hz sampling interval by PC based data acquisition system, which is used in thermocapillary experiment. The each peak intensity (amplitude of temperature change) was obtained by FFT analysis. The relative peak intensities at each frequency (1Hz – 9Hz) were plotted as shown in Fig. 2-4. This result showed variation of measured amplitude was ±2dB. Fig. 2-4 also shows higher frequency response (up to 40Hz). The results showed enough performance for thermocapillary experiment.

Numerical simulations revealed existance of multi-frequency components of temperature fluctuation at oscillatory flow [3]. Frequency separation performance was tested using measuring object, which can simulate surface temperature fluctuation with two frequency components.

Figure 2-5 shows experimental set up. A measuring object was tungsten halogen lamp

whose lighting intensity was controlled with time dependent change. A wave generator, which makes it possible to output synthesized sinusoidal wave with two-frequency components, was used. The frequency components consisted of fundamental frequency (0.25Hz: average value of experimentally observed oscillatory flows) and superimposed frequency (~5Hz: maximum responsive frequency of light source). The amplitude of fundamental frequency component was set to about 1K by controlling the amplitude of synthesized wave (the amplitude of superimposed frequency component was set to about 0.5K.). Figure 2-6-A and 2-6-B show typical synthesized wave and power spectrum of lighting intensity measured by radiation thermometer (frequency components of temperature fluctuation: 0.25Hz and 5Hz). The power spectrum clearly shows two frequency components of 0.25Hz and 5Hz. The superimposed frequencies lower than 5Hz were clearly separated from fundamental frequency. It is concluded that the radiation thermometer has capability to detect multi-frequency components of temperature fluctuation at oscillatory flow.

2.1.3 Amplitude of Temperature Fluctuation

Amplitude of surface temperature fluctuation of oscillatory flow is one of the important physical value. In order to verify the amplitude of temperature fluctuation measured by the radiation thermometer, simultaneous measurement was performed using an unsheathed thermocouple with fast response prepared for ultra high vacuum product (Fig. 2-7). Figure 2-8 shows the measuring position of thermometers. The actual surface temperature fluctuation of oscillatory flow was measured with measuring object for verifying the amplitude. Under oscillatory flow, periodic temperature fluctuation with some phase difference (amplitude is equal) was sometimes detected by two radiation thermometers positioned at different direction. If this temperature fluctuation is measured with radiation thermometers and thermocouple simultaneously, the validity of measuring amplitude is to be verified. The capability of non-contact measuring technique using thermocouple was also examined in this experiment. The measuring junction of thermocouple was carefully approximated to liquid bridge surface at oscillatory flow (oscillatory flow was confirmed by output signal of radiation thermometer.). Temperature fluctuation was not observed by thermocouple even if output signal was amplified (maximum gain: ×50000) at the minimum clearance (50ìm:clearance between measuring junction of thermocouple and liquid bridge surface). It was confirmed that thermocouple could not be applied for non-contact measuring. Figure 2-9 shows the temperature fluctuation of actual oscillatory flow measured with two radiation thermometers and the thermocouple contacted to the surface. Just after the measuring junction of thermocouple contacted to the liquid bridge surface, output signal of the radiation thermometers dropped about 0.5K and frequency of temperature fluctuation was also lowered (about 50% of before) by heat loss and drug force. After this, all amplitude and frequency of temperature fluctuation became almost equal. This result showed the amplitude measured with the radiation thermometers was appropriate. It was also confirmed that frequency of temperature fluctuation was strongly affected by small object, which was contacted to fluid surface.

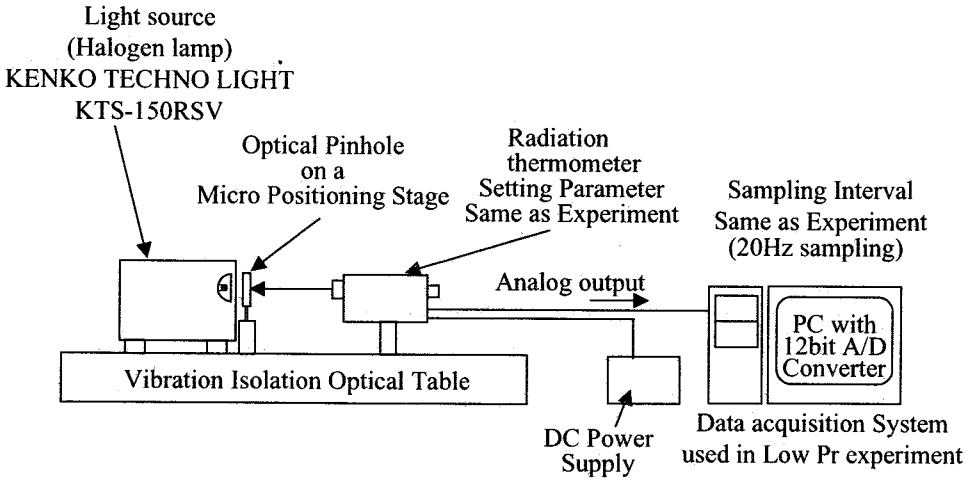

Fig. 2-1 Experimental set up for measuring spatial resolution of radiation thermometer

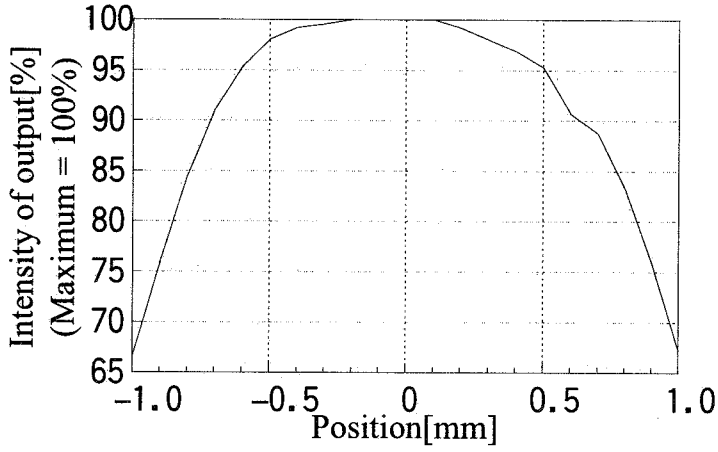

Fig. 2-2 Measuring results of spot diameter

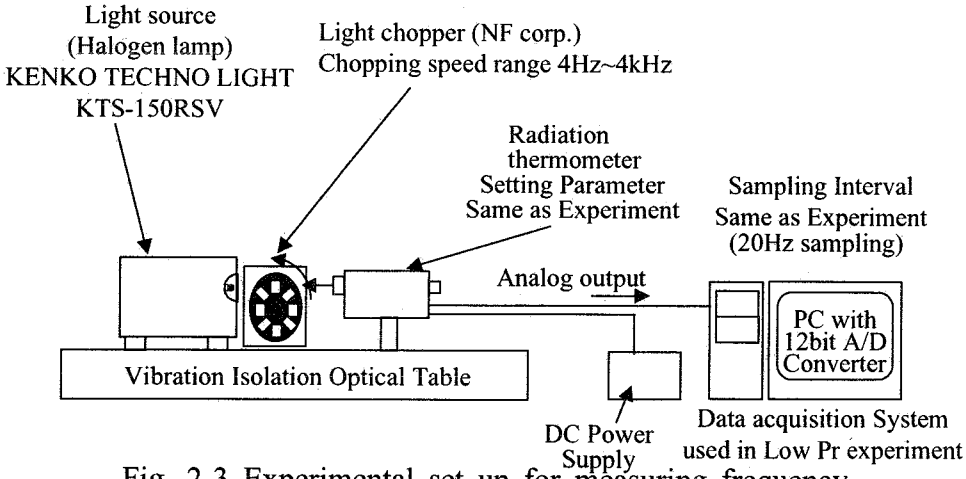

Fig. 2-3 Experimental set up for measuring frequency response of radiation thermometer

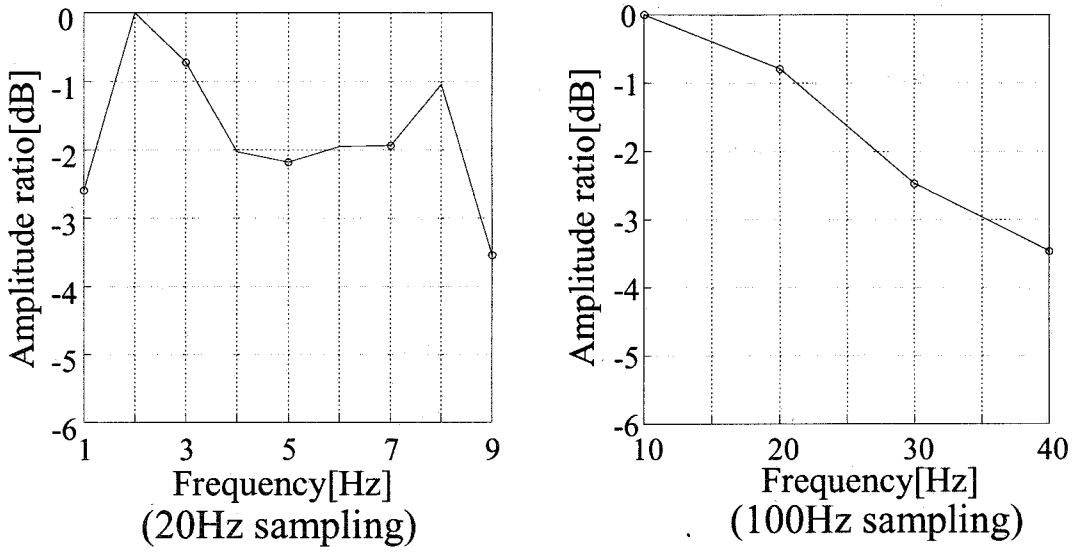

Fig. 2-4 Frequency response of radiation thermometer

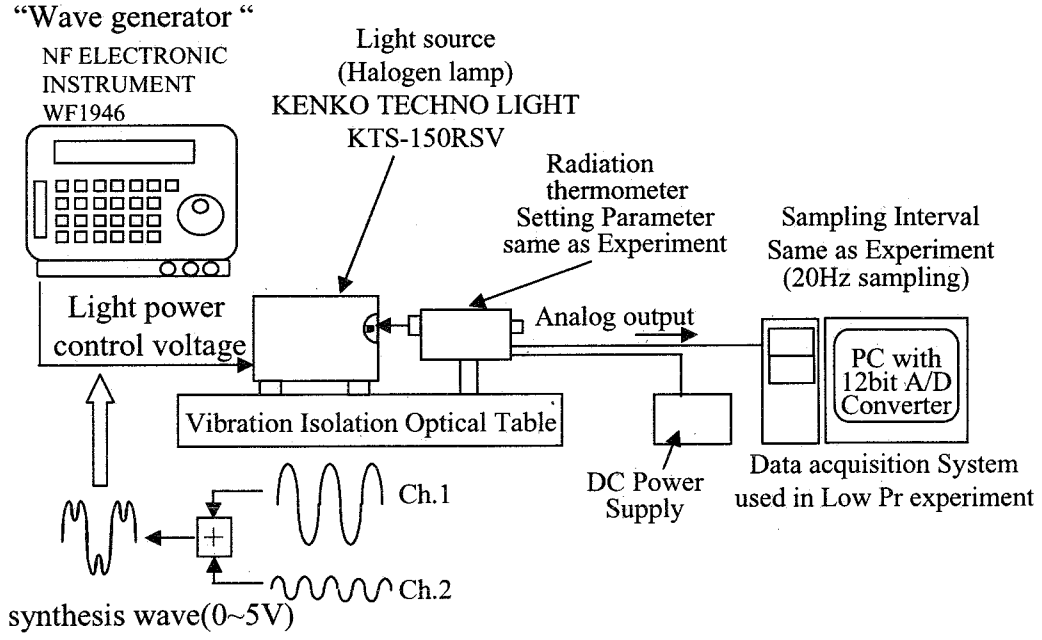

Fig. 2-5 Experimental set up for verifying frequency response of radiation thermometer

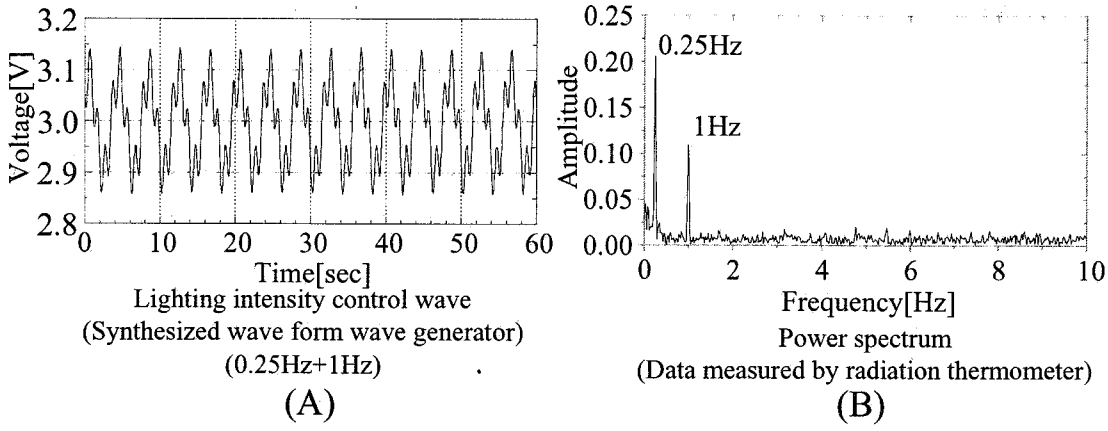

Fig. 2-6 (A)Lighting intensity control waveform and (B)power spectrum of measuring data

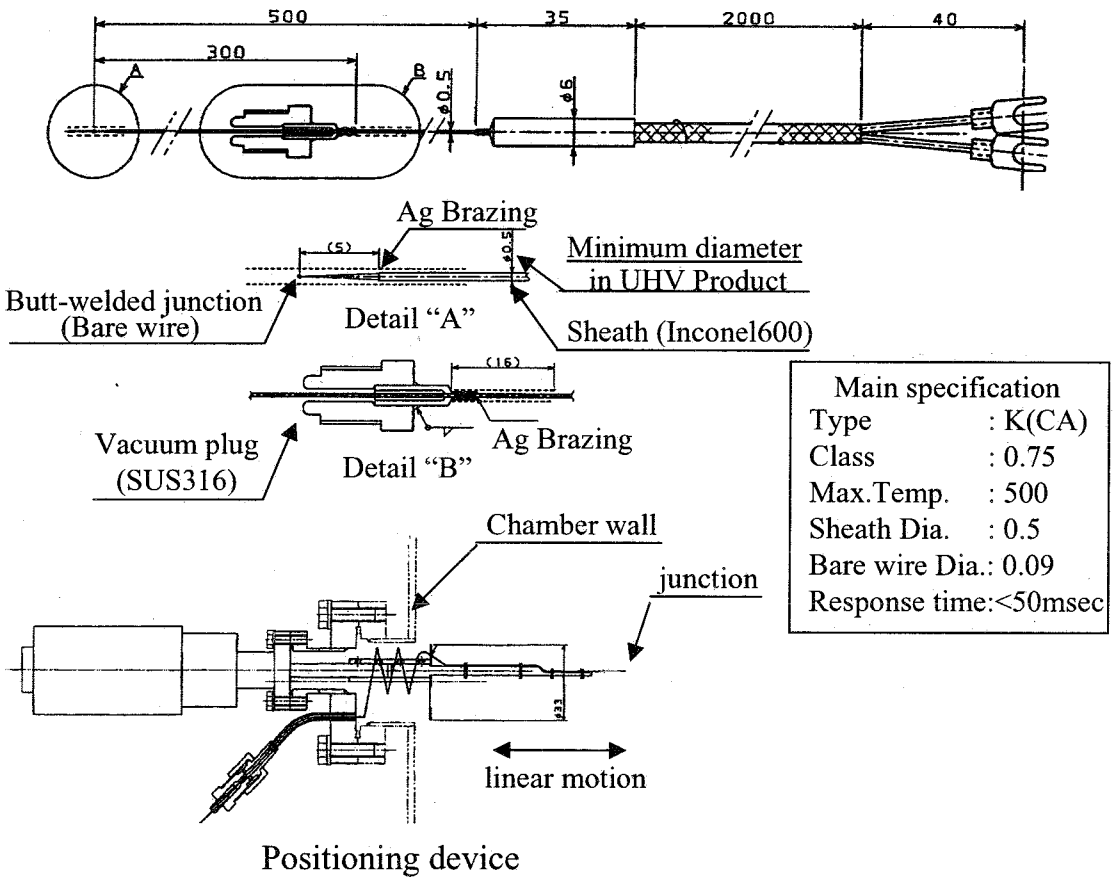

Fig. 2-7 Unsheathed thermocouple prepared for ultra high vacuum conditions

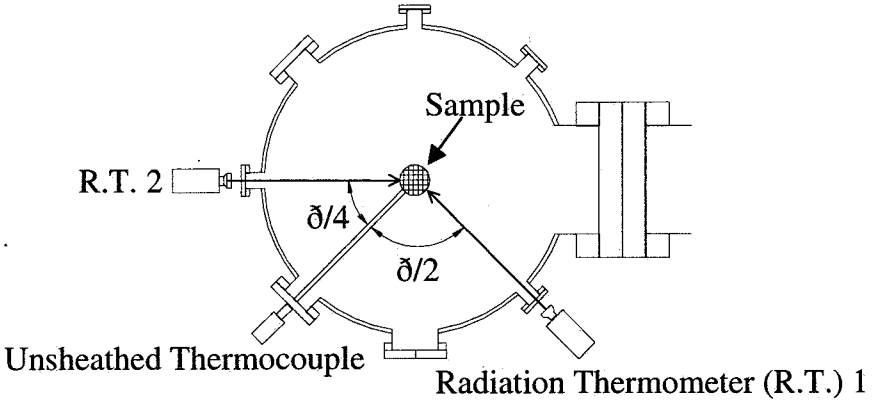

Top view of test section

Fig. 2-8 Measuring position of thermometers

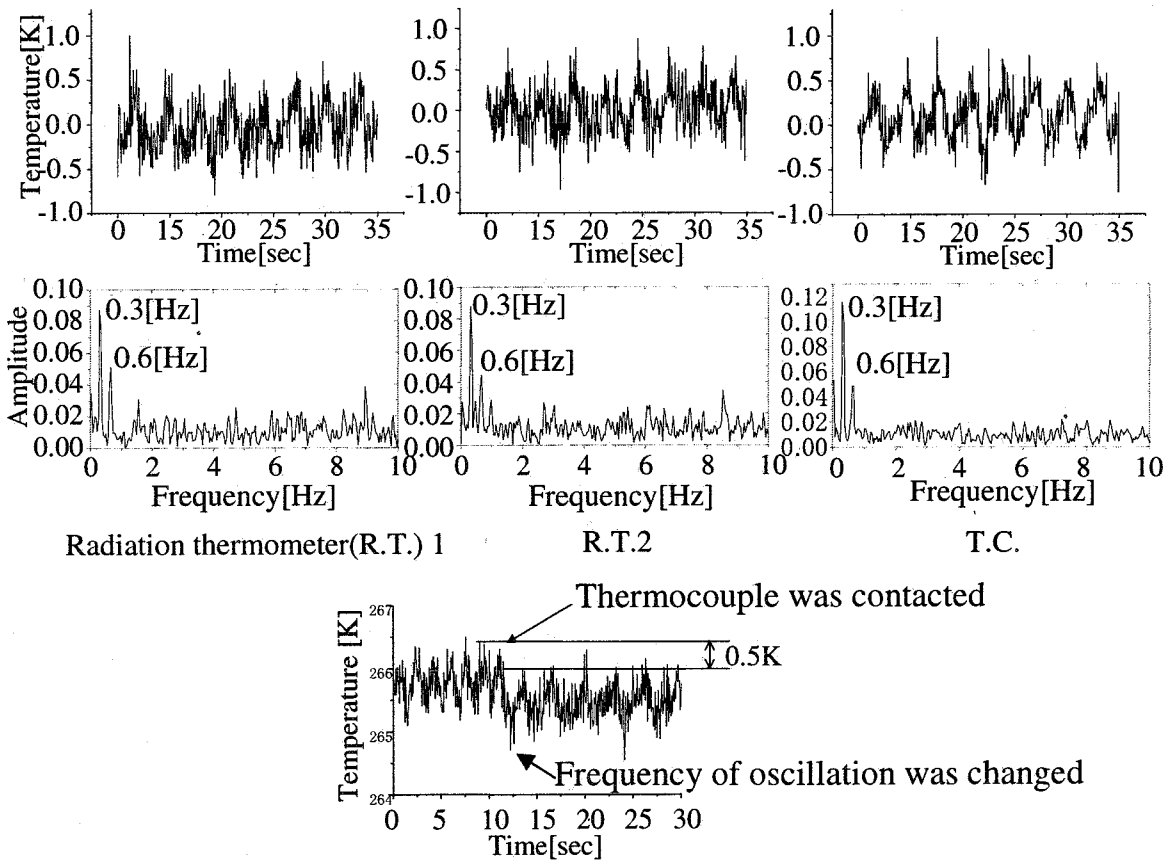

Fig. 2-9 Surface temperature fluctuation of actual oscillatory flow measuring by thermometers

2.2 Detection of Transition Phenomena to Oscillatory Flow

A surface temperature fluctuation of molten tin was successfully observed with the radiation thermometer as shown in Fig. 2-10. The specimen was a liquid bridge of 1.5mm in radius and 2.02 in aspect ratio (As: height/radius). The initial temperatures of the upper and lower disk were 630 and 632K, respectively ($\Delta T = -2K$). The final temperatures of them changed to 616 and 588K, respectively, by the gas cooling of the lower disk ($\Delta T = 28K$). The average changing rate of ΔT ($d\Delta T/dt$) was 0.022K/s. Temperature fluctuations of two points of the liquid bridge surface (measuring area: about 1mm-ϕ) were measured around the center of the bridge height. Since the liquid bridge was slightly deformed by gravity, leading to a difference in radiation energy that can detect by each thermometer, and no correction was made by using the proper emissivity for both thermometers (emissivity: 0.1 for both), absolute temperature values were not the same and not in accord with the real temperature of the liquid bridge. However, it should be noted that the important information is not the absolute temperature but a relative fluctuation component in this study.

The minimum amplitude of the temperature fluctuation was 0.5K in the FFT analysis region as shown in Fig. 2-10-A, which is sufficiently larger than the temperature resolution (0.24K [9]). This fluctuation observed at around 1030sec which corresponded to ΔT=9.1K and Ma=43.3 ($\sigma_T = -0.9\times10^{-4}$ N/mK, $\mu = 1.4\times10^{-3}$ Pas, $\alpha = 2.0\times10^{-5}$ m^2/s). The frequency of the temperature fluctuation was about 0.08Hz near the onset point and then gradually increased (Fig. 2-10-A). In the middle ΔT region, there were some frequency components at around 0.3-0.5Hz (Fig. 2-10-B). After that, the fluctuation behaved as a standing wave of 0.42Hz with a very strong amplitude (Fig. 2-10-C). Re-analysis of this standing wave by FFT with a 2.5Hz low-pass filter revealed the existence of a 0.9Hz component as shown in Fig. 2-11.

It can be concluded that the temperature fluctuations presented here were not caused by external disturbances but caused by the transition to 3D oscillatory Marangoni flow. Validity of the experimentally determined Ma_{c2} and the frequency of the standing wave were discussed and confirmed by comparing with a numerical result [10].

The present results clearly suggest that the transition to oscillatory Marangoni flow was quantitatively detected by the surface temperature fluctuation measurement. Furthermore, we confirmed the transition by flow visualization with tracking slag movement on the liquid bridge surface. Molten tin pre-mixed with a small amount of the slag particle (tin-oxide) was carefully fed onto the lower rod. Since wettability between the slag and the melt is low and density of the slag is lower than the melt, all the particles exist substantially on the surface near the upper rod at ΔT=0 or less. However, when $+\Delta T$ was imposed, the particles quickly moved down, which showed clearly the existence of downwards flow by Marangoni convection. Figure 2-12 shows the movement of the particles obtained from a video image before and after the onset of the oscillation (a=1.5mm, As=2.29, $d\Delta T/dt = 0.018$ K/s). The upper particles repeated in an oscillatory movement along circumference direction with 0.5sec interval and velocity of about 1.2mm/s. It is concluded that the slag particles moved by pulsating oscillatory thermocapillary flow and that there was an apparent critical ΔT between 7 and 8K. Therefore, the transition was directly verified by this surface flow visualization experiment.

The transition phenomena to oscillatory thermocapillary flow in a low Pr fluid, which has never been observed by a non-contact measurement so far, was successfully detected by those quantitative experiments under normal gravity. However, a liquid bridge geometry in which a gravity effect on thermocapillary flow, especially on a static deformation of the bridge shape, is negligibly small is limited to only a lower height of the bridge (lower than about

2.5mm for a molten tin column) [12]. In the next section, we present the results conducted with the smaller liquid bridges in order to avoid the gravity effect which makes an effect of aspect ratio on the critical condition to oscillatory thermocapillary flow uncertain. It should be noted here that there is a same limitation in a liquid bridge size for a low Pr fluid experiment under normal gravity in general.

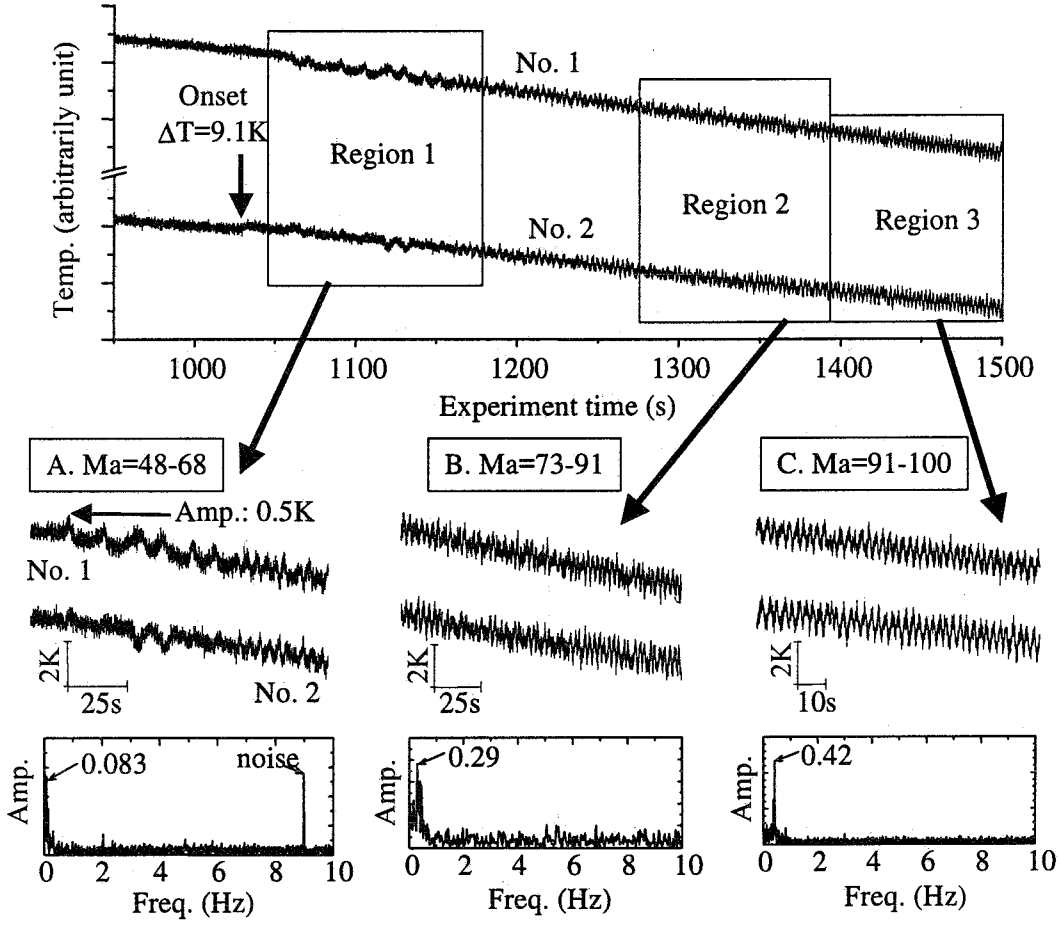

Fig. 2-10 Surface temperature fluctuations of the molten tin column (a=1.5mm, As=2.02). Overall features and enlarged features in A, region 1, B, region 2, and C, region 3 with power spectrum.

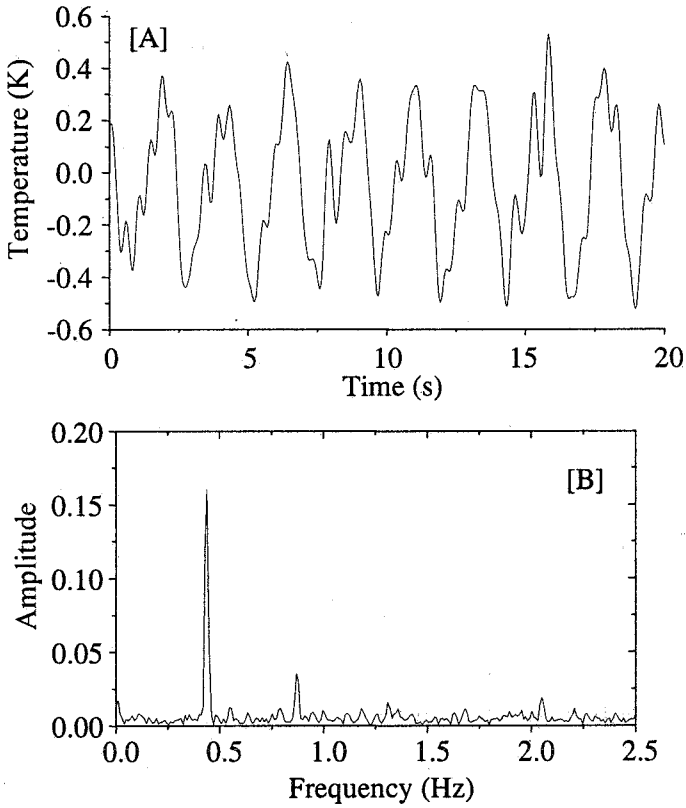

Fig. 2-11 FFT analysis of the standing wave shown in Fig. 2-10-C with 2.5Hz low-pass filter. A. Waveform, B. Power spectrum.

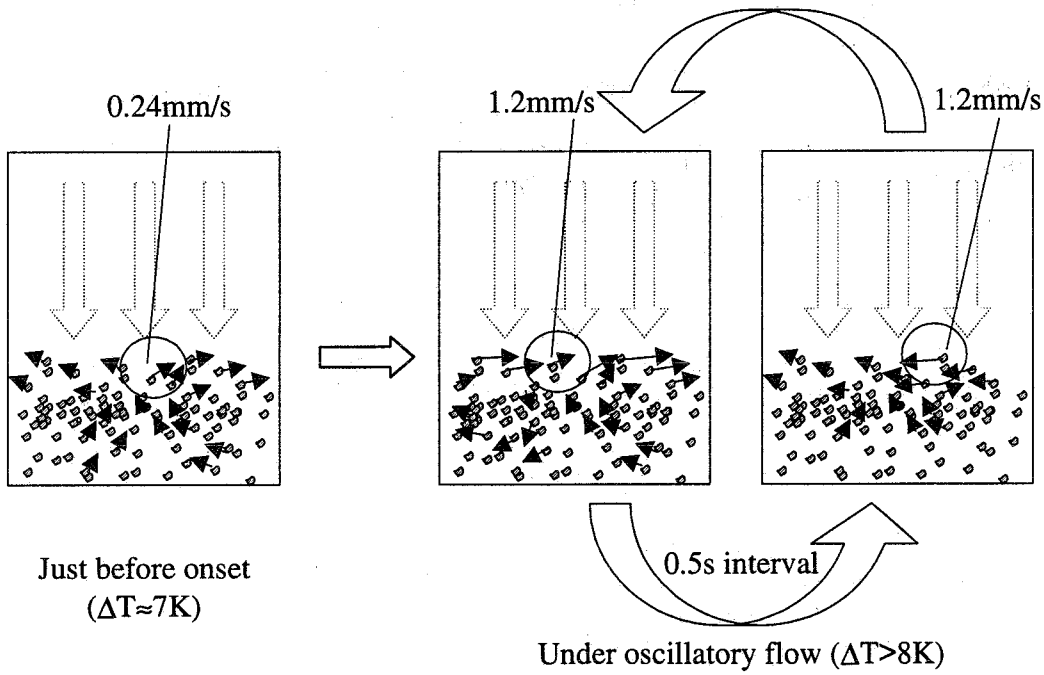

Fig. 2-12 Surface flow visualization by tracking movement of the slag particles before and after the onset of oscillation.

2.3 Mac2 as a Function of As

In order to clarify Ma_{c2} as a function of As, surface temperature measurement using liquid columns with As from about 0.8 to 2.2 is currently under studying.

The disk radii of 1.5~3.0 mm were used. Heights of the liquid column were carefully adjusted in order to minimize the Bd (Bd<1). The $d\Delta T/dt$ was also changed to study the relationship between Ma_{c2} and the observation time as previously mentioned. The performed experimental conditions are summarized in Table 2-1.

The Ma_{c2} as a function of As, which was experimentally and numerically obtained by Imaishi *et al.* [13], are shown in Fig. 2-13. However the experimental Ma_{c2} in the range of As higher than about 1.4 well corresponds to numerical one, that in the range of As less than about 1.3 has scattering within a factor of 1.5. The experimental Ma_{c2} increases with decreasing of As in the range of $As \leq 1.24$. In contrast, the numerical Ma_{c2} has a peak at As=1.2 and the one slightly decreases when As in the range of $1.0 \leq As \leq 1.2$ decreases. The experimental results showed that the Ma_{c2} ($As \leq 1.3$), which was obtained using the liquid column with relative large radius and the one lied on relative low Marangoni number, was obtained by the experimental conditions at small $d\Delta T/dt$. Since the enough experimental data has not been obtained in the range of $1.4 \leq As < 2.0$ and the scattering exists due to the observation time in the range of $1.0 \leq As \leq 1.24$, more detailed study is necessary to clarify Ma_{c2} as a function of As.

Table 2-1 Experimental conditions

a (mm)	As (-)	$\lvert d\Delta T/dt \rvert$ (K/s)	Bd (-)
3.00	0.87~1.24	0.005~0.052	0.46~0.94
2.50	1.07~1.39	0.006~0.034	0.49~0.82
2.25	1.03~1.10	0.022~0.057	0.37~0.42
1.50	1.38~2.02	0.013~0.025	0.29~0.63

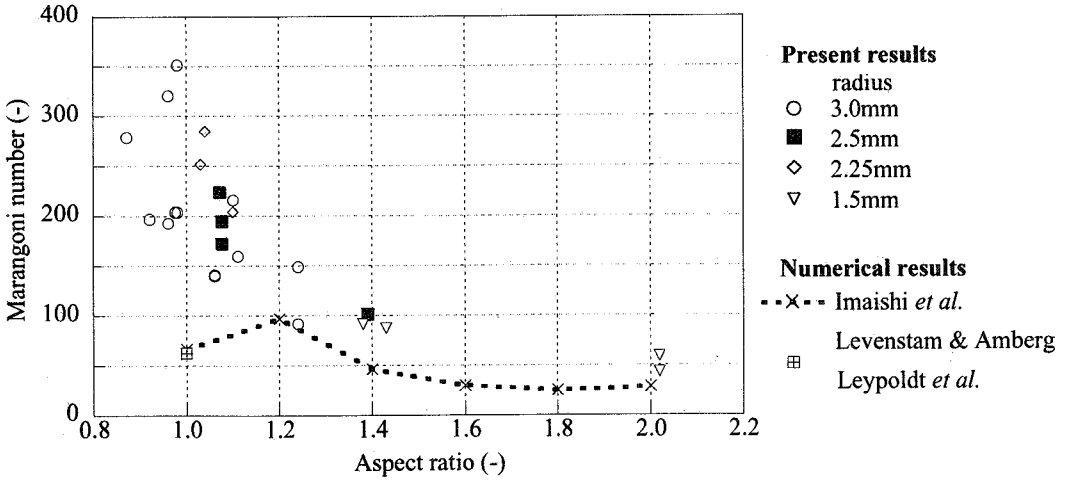

Fig. 2-13 Ma_{c2} as a function of aspect ratio

2.4 Speculation of Internal Temperature Field

The internal temperature fields of liquid bridge were speculated by an analysis of phase difference in surface temperature fluctuations. The typical two experimental cases (Case1: As=2.02, Case2: As=1.45) were studied. The measuring positions of each experimental case were illustrated in Fig. 2-14.

Figure 2-15 shows the analyzed waveforms of surface temperature fluctuation and speculated internal temperature field.

Both waveforms of case1 show that frequency is almost same (FFT results: 0.42Hz). It also shows that phase difference is about 180degree. In the case2, the frequencies of three waveforms are also equivalent (FFT results: 0.03Hz). Temperature3 (red line in figure, measured by radiation thermometer No.3) is ahead of temperature1 (black line in figure, measured by radiation thermometer No.1) with slight phase difference. Phase difference between temperature 1 and 2 (green line in figure, measured by radiation thermometer No.2) is almost 180degree. From analyzing waveforms as mentioned above, if hot or cold region was locally generated and fluctuated with azimuthal wave number (m) same as flow field predicted by numerical simulation [3]and [14], internal temperature field (horizontal cross section) of liquid bridge could be speculated as shown in Fig. 2-15.

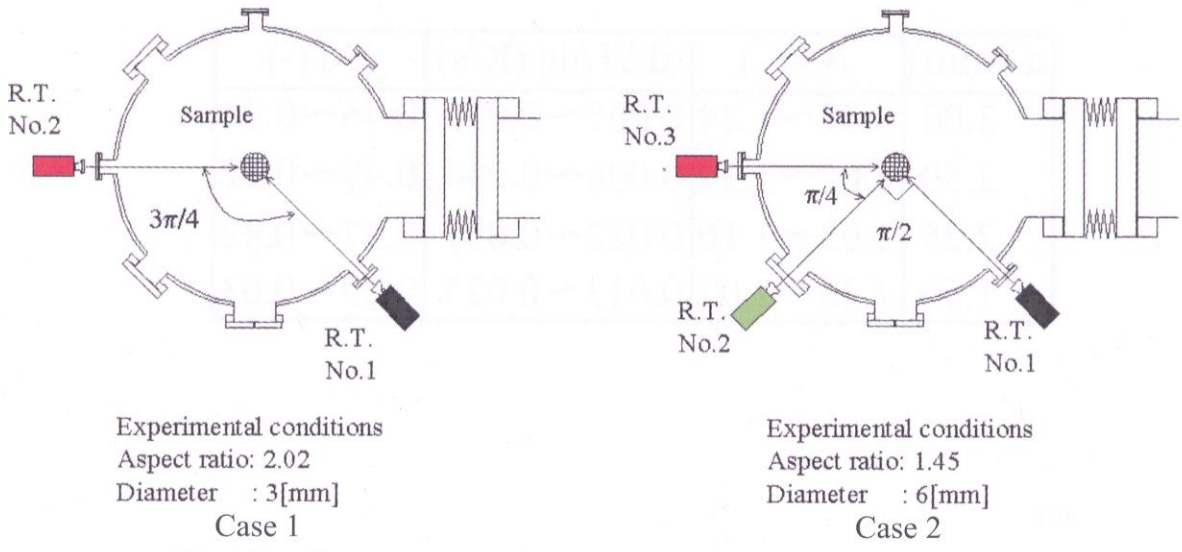

Fig. 2-14 Measuring position of radiation thermometers

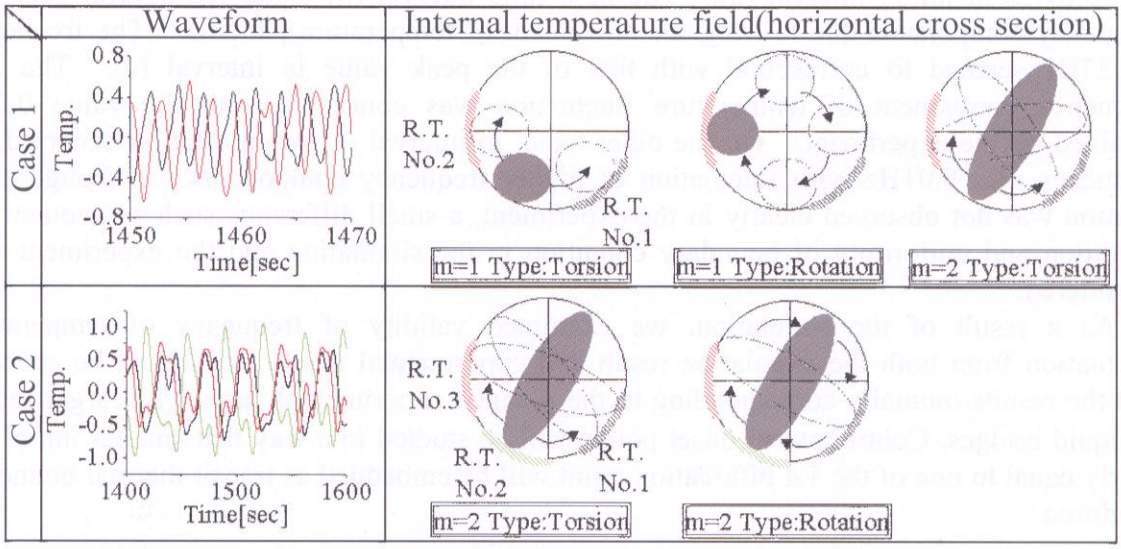

Fig. 2-15 Analyzed waveform and specurated internal temperature field

2.5 Numerical simulation

The numerical simulation was performed under the same condition as the experiment. The objective of this simulation was to check the onset point and the surface temperature behavior depended on time obtained by the experiment. The simulation program was developed by Prof. Imaishi and Dr. Yasuhiro, and modified by Dr. Yasuhiro so that we could deal with transit thermal boundary conditions, dimensional data convenient for direct comparison with experimental data and natural convection in 1G.

A size of the liquid bridge to be analyzed was specified in the experiment case in which radius a=1.5mm and height h=2.97mm was employed, thus aspect ratio As=1.98. According to the experimental result, onset of temperature fluctuation was observed when temperature difference ΔT of hot and cold iron disks became 9.1K. Figure 2-16 shows fitting value of imposed ΔT. Horizontal axis represents experimental time. In order to confirm the onset of temperature fluctuation, initial ΔT was set enough small value 5.99K (t=873sec) in the simulation.

Figure 2-17 shows the simulated surface temperature at local points of middle height of the liquid bridge. Temperature fluctuation was observed at t=881sec (ΔT=6.2K) after 5sec interval of 3D-steady state. The onset appeared earlier than that of experiment (t=1090sec, ΔT=6.2K). The temperature fluctuation pattern changed with progress of time. Figure 2-18 shows typical temperature distribution in the cross section r-θ plane at the middle height of the liquid bridge. In the time interval from t=883 to 895sec, two patterns appeared alternately. One was the pattern that two hot regions appeared in the opposite side of surface of liquid bridge, and another was that one hot region appeared in the middle point of described two hot surface regions. Hot and cold regions of two patterns corresponded to the positions where $\theta=\pi/2$ and π. The fluctuation was clearly observed in the alternation of the surface temperature in figure 2-17. These alternative patterns moved azimuthal direction irregularly after t=895sec. Further more time progress from t=924sec, they became to rotate.

Result of FFT analysis for each time interval temperature data was shown in figure 2-19. Each of them corresponded to the described pattern. Dominant fluctuation component value

is f=0.29Hz in initial interval (a). The next time interval (b) contained several peaks of frequency components due to irregular movement of temperature patterns. The frequency f=0.27Hz seemed to correspond with that of the peak value in interval (a). The low frequency component of temperature fluctuation was consistent with the value 0.2Hz obtained by the experiment. On the other hand, in interval (c) when rotation occurred, its frequency was 0.01Hz with fluctuation of higher frequency components. Although such rotation was not observed clearly in the experiment, a small difference such as geometrical condition and uniformity of boundary condition in the simulation and the experiment was considered.

As a result of the simulation, we examined validity of frequency of temperature fluctuation from both the simulation result and experimental result. It should be checked that the results mutually corresponding to the planned experimental cases with larger radius of liquid bridges. Contrariety of onset points will be studied in a way that smaller initial ΔT nearly equal to one of the 1st bifurcation point will be embedded as transit thermal boundary condition.

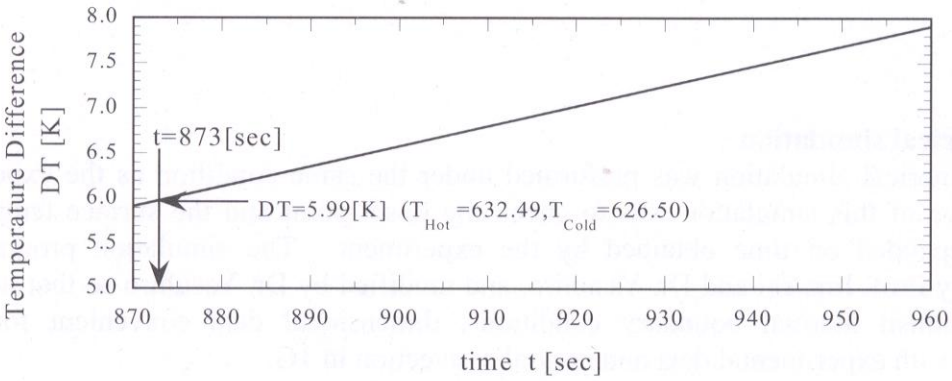

Fig. 2-16 Imposed temperature difference

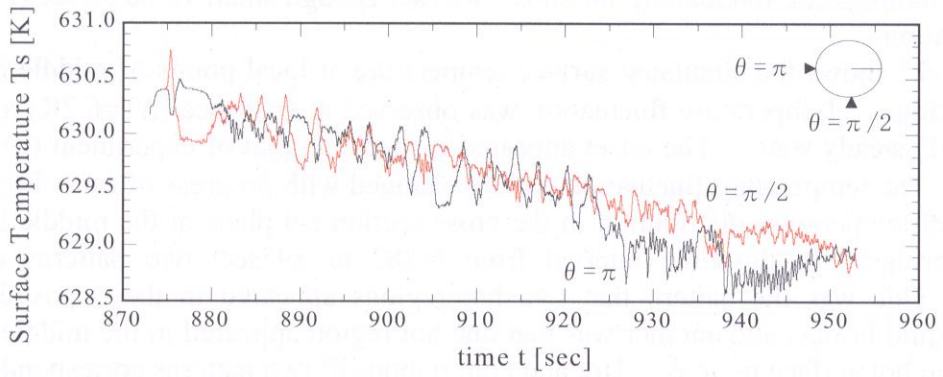

Fig. 2-17 Surface temperature fluctuation (As=1.98, a=1.5mm , Pr=0.08, g=9.8m/sec^2)

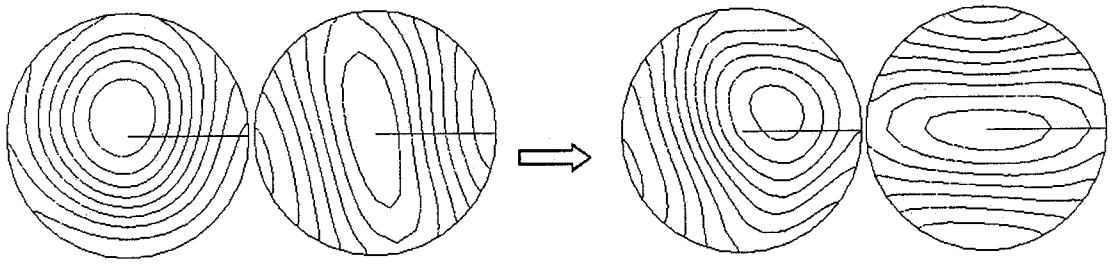

(a) t=883 - 895sec (b) t=896 – 924sec

Fig. 2-18 Patterns of temperature distribution in cross section at middle height

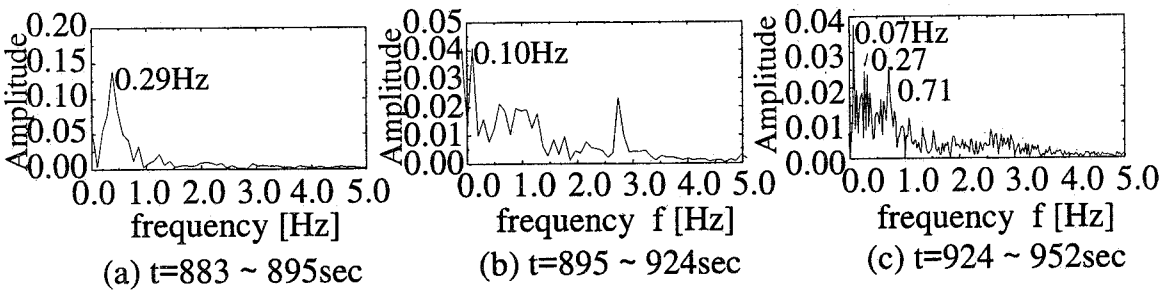

Fig. 2-19 Power spectrum (è=ð/2)

3. OXYGEN PARTIAL PRESSURE DEPENDENCE OF SURFACE TENSION OF MOLTEN TIN

Mukai *et al.* [15] presented changes in surface tensions (σ) and its temperature coefficient (σ_T) of molten silicon with changing ambient oxygen partial pressures (P_{O2}). The values of σ and σ_T were strongly dependent on the P_{O2} ranging from 10^{-25} to 10^{-14}MPa. Since there were only a few data of σ and σ_T of molten tin measured at a clearly defined P_{O2} [16] and the reactivity of molten tin toward oxygen is similar to that of molten silicon, an oxygen partial pressure dependence of σ and σ_T of the melt should be studied at around the temperatures of the thermocapillary experiment. Last year, the actual values of σ in our experiment chamber were measured, which led us to estimate of the actual P_{O2} at the outlet of the chamber [9], *i.e.* in the order of 10^{-9}Pa. In this year, quantitative relations among the surface tension of molten tin, an ambient P_{O2}, and temperature are systematically studied with the surface tension measurement apparatus specially designed for molten tin in which a P_{O2} can be controlled below 10^{-14}Pa in an Ar gas flow. A detail of experimental method and a thermodynamic analysis were presented in the literature [16].

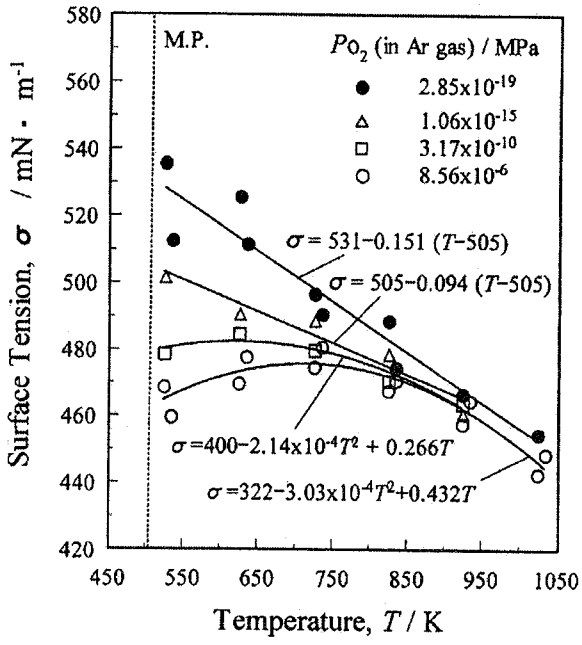

Fig. 3-1 Temperature dependence of the surface tension of molten tin in the temperature range from 523 to 1033K

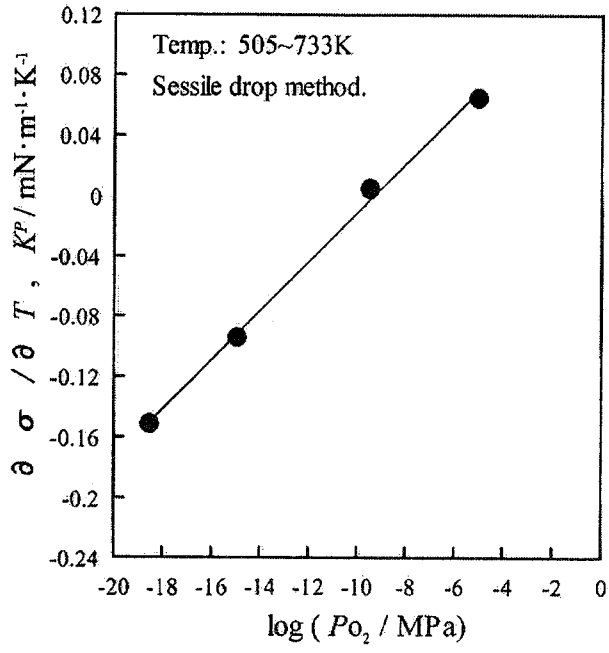

Fig. 3-2 Temperature coefficient of surface tension of tin as a function of oxygen partial pressure

The surface tension of molten tin was measured at various temperatures between 523 and 1023K under P_{O2}=2.85x10^{-19}, 1.06x10^{-15}, 3.17x10^{-10}, and 8.56x10^{-6}MPa (average value) in the purified argon gas flow. The results are summarized in Fig. 3-1. The temperature coefficients of surface tension, $(\partial\sigma/\partial T)_{P_{O2}}$, were found to be –0.151 and –0.094 mN/m/K for P_{O2} of 2.85x10^{-19} and 1.06x10^{-15}MPa, respectively, which are within the values reported by the various investigators (–0.02 to –0.22) [16]. However, $(\partial\sigma/\partial T)_{P_{O2}}$ increased with growing the P_{O2}, and in case of the P_{O2} above 3.17x10^{-10}MPa, it finally changed from minus to plus value around at the melting point of tin whose temperature is below 733K. It is concluded that the sign of the temperature coefficient of molten tin surface tension changes depending on an oxygen partial pressure of a surrounding gas. Figure 3-2 shows the relation between $(\partial\sigma/\partial T)_{P_{O2}}$ and log P_{O2} near the temperatures of thermocapillary experiment. It is clear that $(\partial\sigma/\partial T)_{P_{O2}}$ increased with growing P_{O2} and the sign of the coefficient changed from minus to plus at about log P_{O2}= –9.375MPa. The observed behavior of the surface tension was explained qualitatively [16] based on a model proposed by Passerone *et al.* [17] which incorporates both thermodynamic and kinetic considerations.

A thermocapillary experiment of molten tin is usually carried out at temperatures of 570-770K, and the estimated P_{O2} at the chamber outlet was in the order of 10^{-9}Pa (log P_{O2}= –15MPa). Therefore, it is concluded that an appropriate value of the temperature coefficient of surface tension of molten tin is –0.9x10^{-4}N/mK for the present experiment chamber.

4. DEVELOPMENT OF 3D-UV AND TRACER PARTICLE

4.1 Development of 3D-UV

4.1.1 Performance Test of Transducer at High Temperature Condition

In 1999, a test for evaluating detectability of $LiNbO_3$ (LN) transducer was performed at room temperature using a drilled glass target, which simulated balloon tracers in molten tin. It was predicted that a detectable minimum diameter of tracer was 200-100ìm [9].

In present work, test for evaluating detectability at high temperature condition as same as actual thermocapillary experiment was performed in molten tin. Experimental set-up is illustrated in Fig. 4-1. A hollow shaft that has semispherical tip (outer diameter: 1mm) was used as a target. The thickness of shell was 0.1mm, which was thinner than half-wave length of ultra sonic wave in order to simulate pseudo-balloon tracer. The target was movable along vertical direction in order to check the sensitive variation. A sensor head, which was attached 4 transducers, was positioned at under these targets. The target was positioned in order to align directly above transducers. The depth of molten tin bath was at a distance of 6mm, which was slightly longer than real liquid bridge. Temperature of tin was 723K which is same as thermocapillary experiment. The hollow target was moved vertically about 3mm from the position at a distance of 1mm from surface of sensor head. Position of the solid target was fixed at near the free surface. Figure 4-2 shows example of an echo signal locus. The echoes from vertical moved target were clearly received at approximately equivalent echo intensity over moving distance.

In this experiment, the results showed that high spatial resolution could be obtained in the direction of wave propagation the same at temperature condition as thermocapillary experiment.

Additional tests using solid target (diameter: 1mm) were performed in order to qualify actual advantage of detectability by tracer structure (hollow or solid). The theoretical reflectance value of solid and hollow target (SUS) in molten tin are 0.45 and 1.0, respectively (the hollow target is 5.2dB higher than solid one). The test result clarified that the echo intensity of hollow target was 6dB higher than that of solid target. This means experimental result corresponded to theoretical value. It is concluded that the advantage of detectability of balloon-like structure was experimentally proved.

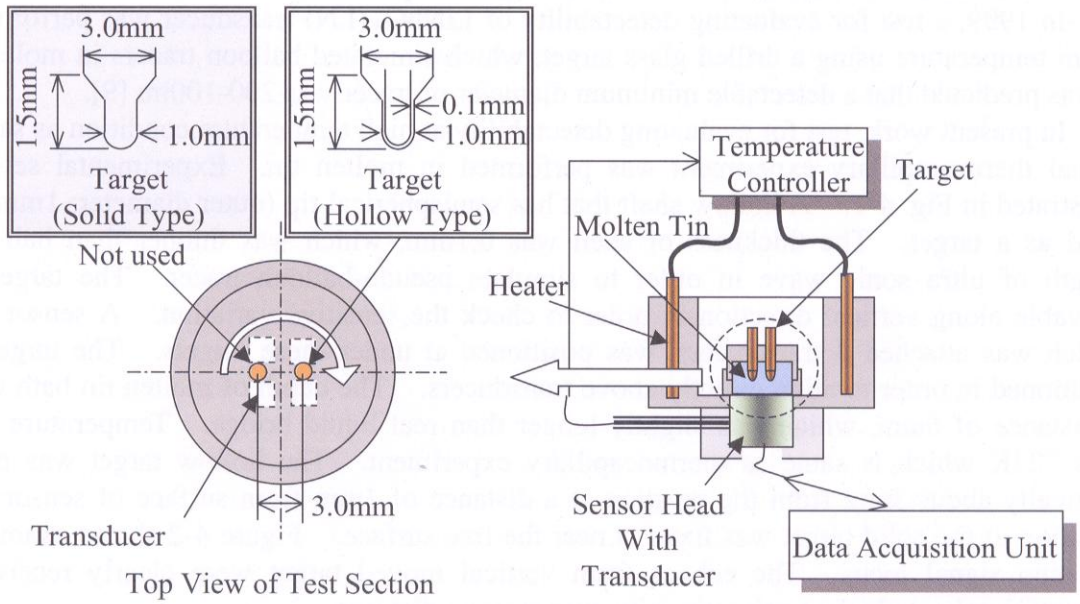

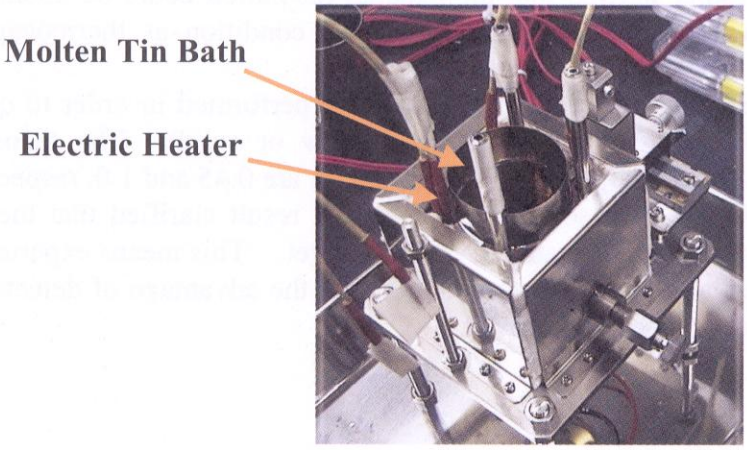

Fig. 4-1 Experimental set up for measuring sensitivity of transducer at high temperature conditions

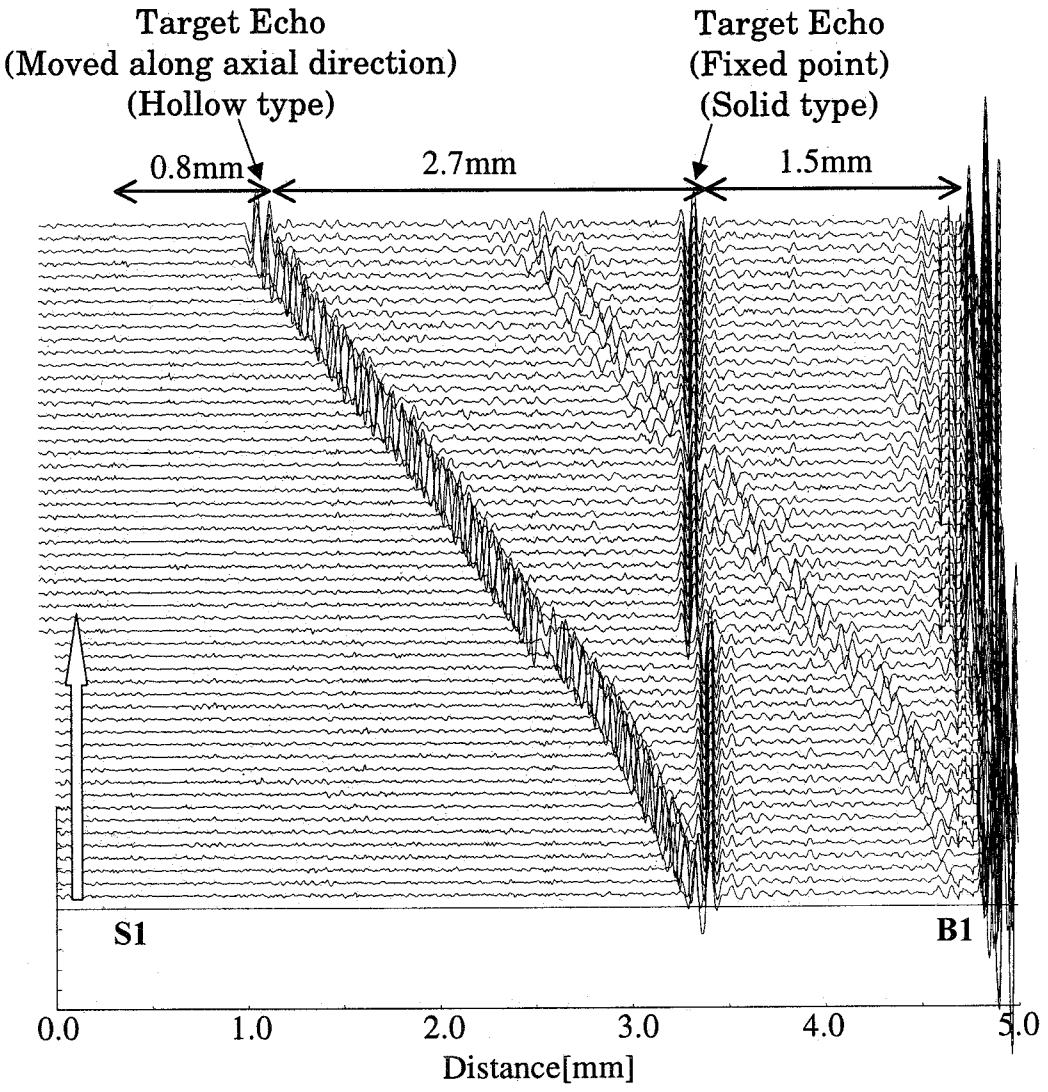

S1 : Echo from Surface(Sensor head – molten tin)
B1 : Echo from Free Surface of Molten Tin

Fig. 4-2 Echo trajectory of moving hollow type target

4.1.2 Evaluation of Visualization Performance

In order to evaluate visualization performance, ultrasonic propagation of tracer in liquid bridge was simulated numerically by using 3-dimensional acoustic analysis program "SOSUM" (Sound Source Superimposed Method) [18]. The numerical scheme used in SOSUM is a kind of boundary element method (BEM). The BEM combined calculation algorism embedded in the program enable high-speed calculation. Sound pressure at any position in analysis domain can be obtained by superposition of sound pressure from sound sources (transducer and reflector of sound).

Table 4-2 summarizes performed calculation conditions. The ultrasonic propagation of two kinds of operating frequency of transducer (Case1: 10MHz, Case2: 20MHz) was calculated in order to evaluate influence of directional angle of transducer due to operating frequency. Figure 4-3 illustrates analysis model in which geometries are based on ongoing sensor design. 27 tracers were fixed in analysis domain of liquid bridge. Since the diameter of real tracer is smaller than wavelength, the each of them can be modeled by one triangle mesh. The tracers were lain on 3 horizontal planes every 9 tracers (bottom plane: Z=0.75, middle plane: Z=2.25, top plane: Z=2.75,). The tracers on a horizontal plane were arrayed at 3×3 matrices like. The boundaries (transducer and surface between sensor head and molten tin) were also modeled by a number of triangle meshes of which size were less than half of ultrasonic wavelength (due to sampling theorem). In order to reduce calculation time, received ultrasonic wave at transducer was calculated by superimposing all sound pressure from sound sources. This means that receiving directivity of transducer was omnidirectional in this simulation. Propagations of ultrasonic waves for all transmitting/reflecting combination of transducers were simulated transiently. Firstly, directivity of transducer was examined by using a transducer and 3 tracers on bottom layer as shown Fig. 4-4. Ultra sound was transmitted by the transducer, which is colored gray as shown in the figure. Value of sound pressure received at the 3 tracers (A, B, C as shown in the figure) were calculated. The relative values (maximum value of sound pressure=1) of sound pressure are summarized in table 4-3. The all values of 10MHz are higher than 20MHz. However the sound pressure of 20MHz received at the tracer C was about 20% of one at the tracer B, sound pressure of 10MHz received at the tracer C was about half of one at the tracer B. The results showed that the directivity of transducer of 10MHz was wider than that of 20MHz, which corresponded to theory. Since the spatial resolution of vertical direction is fine (60ìm at 20MHz, 120ìm at 10MHz), horizontal cross sectional image of traces in liquid bridge was evaluated by visualized results, which were imaged synthetic aperture focusing technique as shown in Fig. 4-5(Case1: 10MHz) and Fig. 4-6 (Case2: 20MHz). The color variation from blue to red in the figure represents intensity of superimposed sound pressure. Position of tracer can be strongly indicated by red color in the figure. In the case1 (10MHz), positions of tracers at bottom and middle planes are indicated by yellow or red region with about 1.0~1.5mm in diameter. However, at top plane, positions of 4 tracers at fringe area are not clear. In the case2 (20MHz), positions of all tracers at 3 planes are relatively clear comparing to those of case1. All tracers are indicated by red region of 1.0~1.2mm in diameter. A theoretical horizontal spatial resolution (ÄX) of sensor with infinitely aperture can be expressed as ÄX=D/2(where, D is an equivalent diameter of transducer). In these cases, ÄX was to be about 1.4mm by using D as diagonally length of transducer. The resolution of both calculation cases corresponded to this theoretical resolution. However, it seems that visualization performance of 20MHz is better than that of 10MHz. The reason of this is as follows. Since the receiving directivity of transducer was not modeled in this simulation as mentioned above, calculated signal intensity of receiving ultrasound at transducer was stronger than real one. These effects increase with growing frequency of transducer. Therefore, intensity of receiving ultrasound

of 20MHz was further overestimated comparing to that of 10MHz. In addition, shorter wavelength of 20MHz contributed to fine visualization performance. From this simulation, it was confirmed that tracers in molten tin liquid bridge could be visualized by both 10MHz and 20MHz transducers.

Table 4-2 Calculation conditions

Case	1	2
Frequency of Transducer	10MHz	20MHz
Size of liquid bridge	6mm(diameter) ×4.5mm(height)	
Size of sensor head (Ti)	20mm(diameter) ×20mm(height)	
Acoustic velocity of Sn	2400m/s	
Acoustic velocity of Ti	5900m/s	
Size and layout of transducer	2mm×2mm, 4×4	
Size of a mesh (Sn)	48×10^{-6}m	
Size of a mesh (Ti)	118×10^{-6}m	
Layout of tracer (horizontal position)	3×3 (arrayed at 2mm distance)	
Layout of tracer (vertical position) 3layer(distance from surface between Ti and Sn)	Top: Z(1) 0.75mm Middle: Z(2) 2.25mm Bottom: Z(3) 3.75mm	

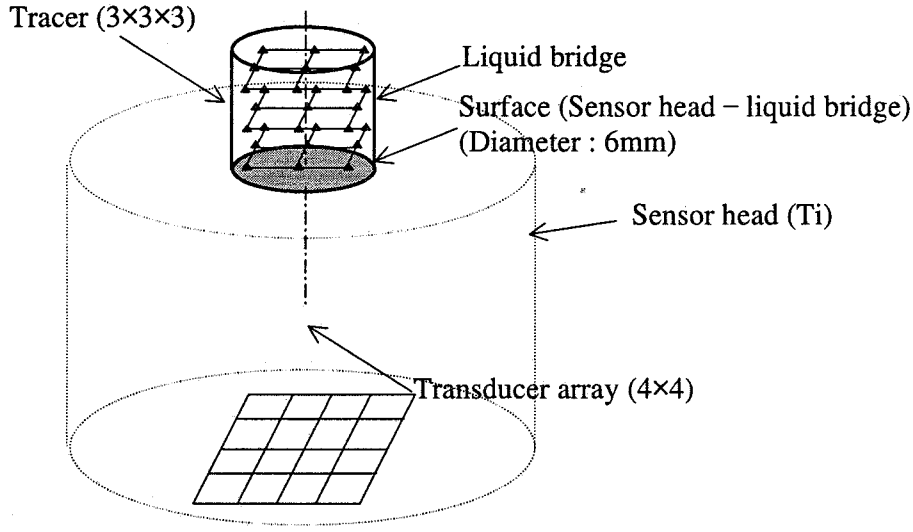

Fig. 4-3 Schematic view of analysis model

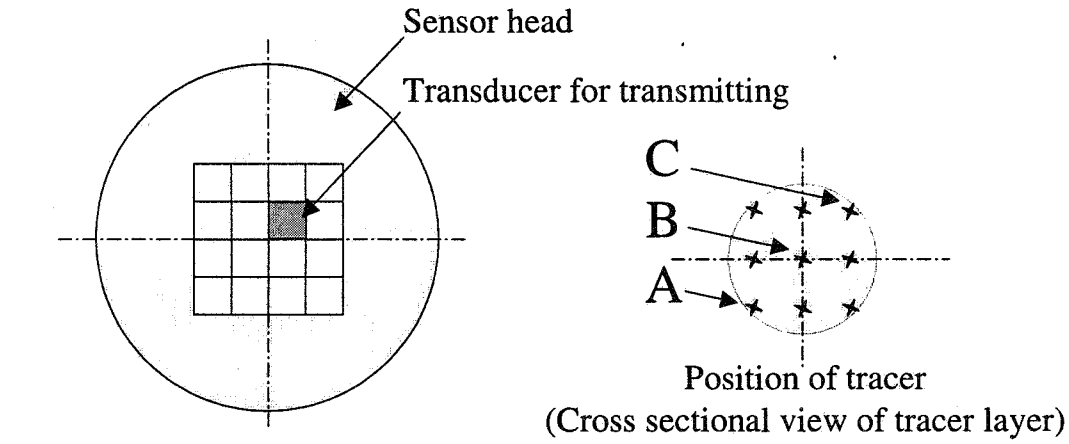

Fig. 4-4 Position of transducer and tracer for evaluating directivity of transducer

Table 4-3 Directivity of transducer

	10MHz	20MHz
Sound Pressure (tracer A)	0.46	0.18
Sound Pressure (tracer B)	1 (Reference)	0.83
Sound Pressure (tracer C)	0.45	0.63

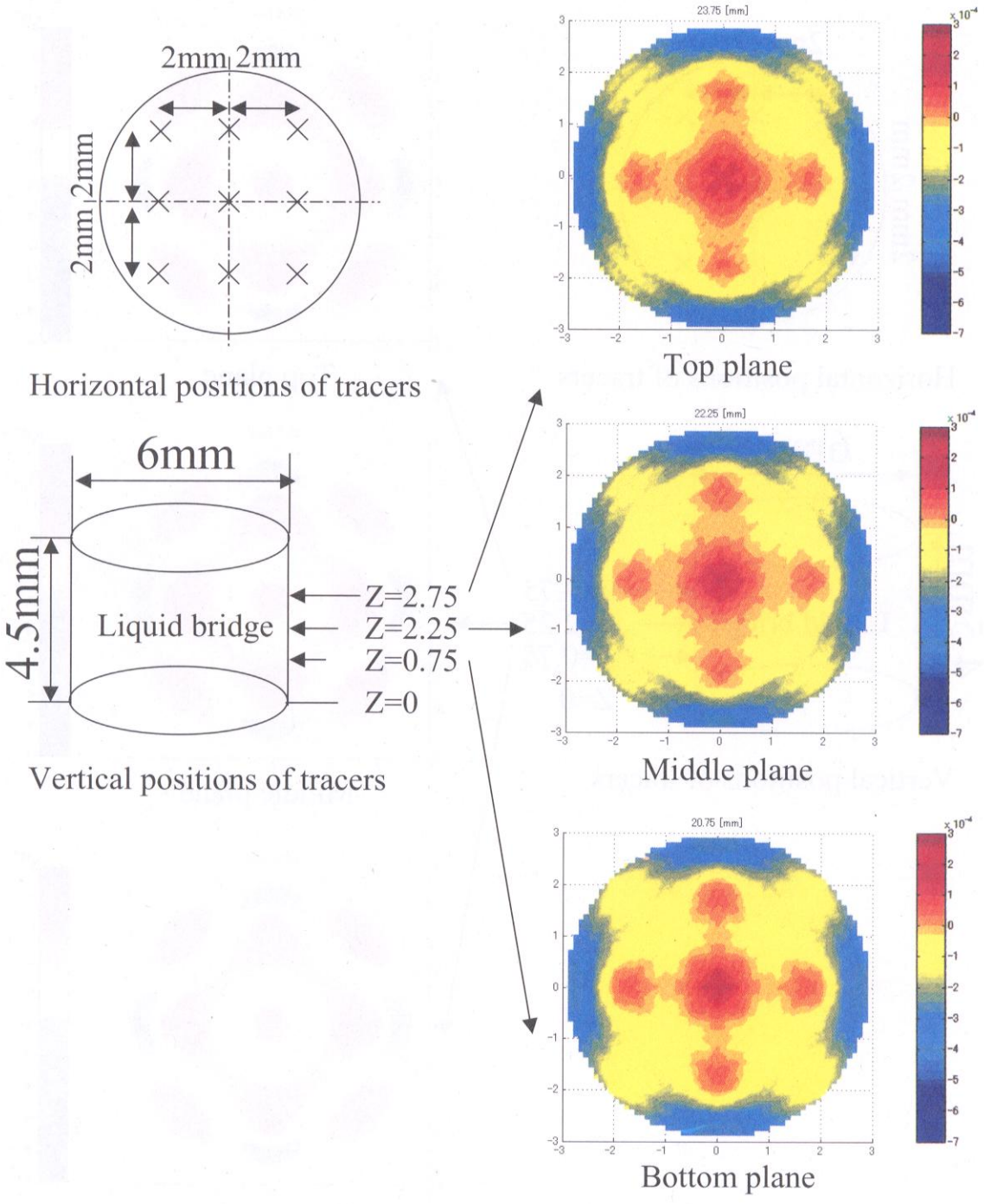

Fig. 4-5 Visualized image of tracer (10MHz)

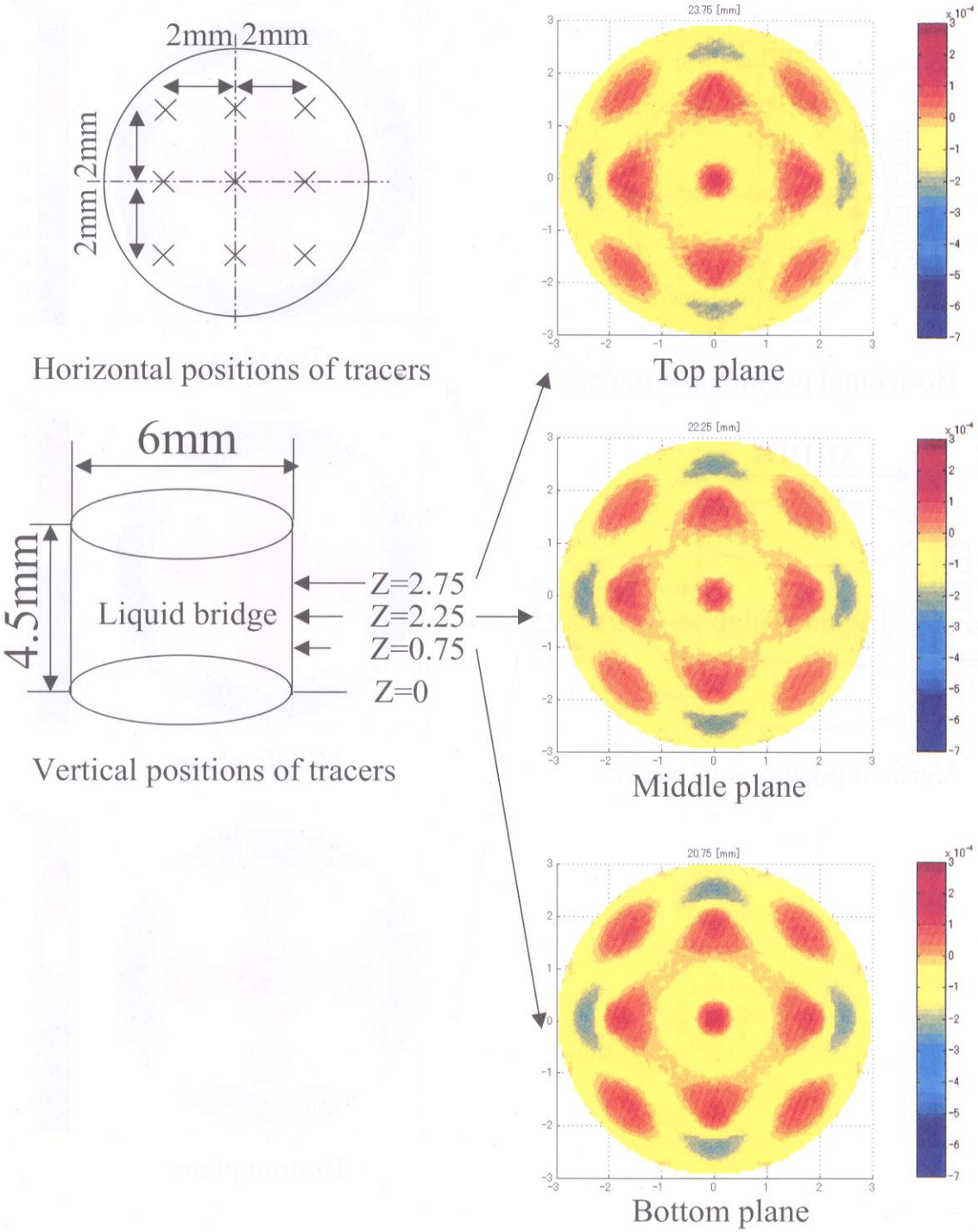

Fig. 4-6 Visualized image of tracer (20MHz)

4.1.3 Design for 3D-UV Measuring Unit

Ongoing design of 3D-UV measuring unit is briefly described in this section.

In order to embed sensor head into supporting disk for liquid bridge, disk assembly with sensor head was designed as shown Fig. 4-7. Since the cooling mechanism was in lower rod, upper rod was selected to embed sensor head.

Figure 4-8 shows conceptual diagram of signal-processing unit. Echo from tracer particle must be received and recorded at the same time by all transducers except for one transducer (using for transmitting). A visualized image of tracer at a moment (objective value: within 10msec) can be obtained by repeating this process several times (=number of transducers). Therefore, each transducer equips pulsar/receiver and fast operating A/D converter which is controlled parallel.

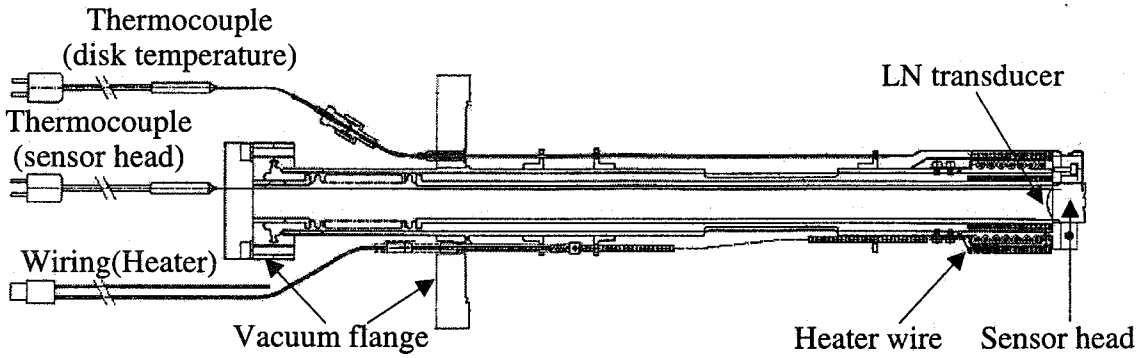

Fig. 4-7 Disk assembly with sensor head

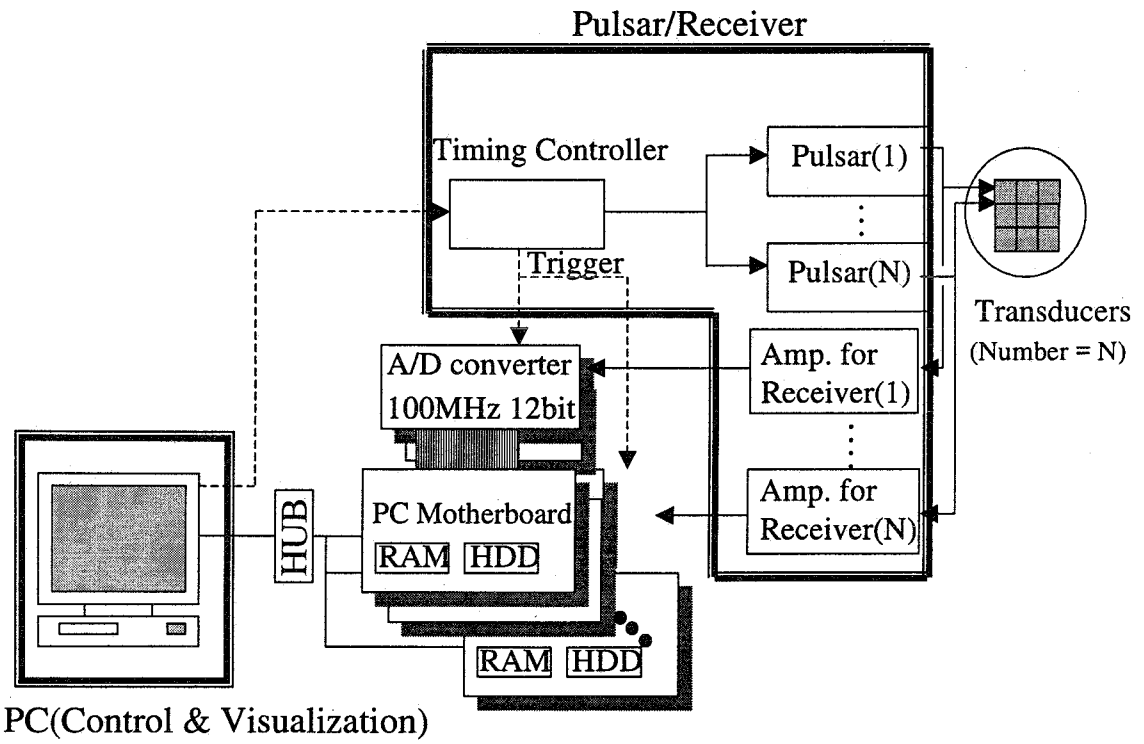

Fig. 4-8 Signal processing unit diagram

4.2 Development of Tracer

4.2.1 Development of Manufacturing Technique

Fe and Ni plated Shirasu-balloons (Fe·Ni/SB) have been developed for tracers of 3D-UV technique [9]. Improvement of sphericity and surface roughness were required for 100ìm-class Ni/SB.

The sphericity was improved by a certain heat treatment technique on Ni plating process. Figure 4-9 shows Ni plated Sirasu balloons (Ni/SB) before and after the heat treatment. However the shape of Ni plated Sirasu balloons (Ni/SB) was not good sphericity before heat treatment, the one became good sphericity with smooth surface after heat treatment. The detailed technique could not be presented here because patent issue is still pending.

The surface roughness was improved on Fe plating process. The Fe plating layer was formed by an electrolysis plating method. The electrodes were pure iron and carbon. The Ni/SB were stirred with brass balls, which were 2mm in diameter, in a plating solution. The plating solution was consisted of two additives. One was saccharin ($C_7H_5NO_3S$). It absorbs on a cathode and suppresses the growth of projections. The other was sodium dodecyl sulfate ($CH_3(CH_2)_{10}CH_2OSO_3Na$). It was used for a remover of hydrogen gas from the surface of Fe plating layer. Figure 4-10 shows the results of improvement of surface roughness. The surface roughness of tracers was improved clearly by the additives.

The Fe·Ni/SB will be exposed heat cycle during the actual thermocapillary experiment. Therefore the following test for Fe·Ni/SB was performed.

In the experiment, tin melt with some Fe·Ni/SB was heated to 670[K] and held for 3.6[ksec.](1hour). After that, it was cooled down to 520[K]. After this sequence, it was heated to 670[K] again and held for 1.8[ksec.](0.5hour). These processes had been done in a quartz tube in which atmosphere was maintained at low vacuum condition (under 10^{-3}[Pa]).

It was confirmed that most of tracers were not collapsed but contained in tin melt after the experiment. The interface of Fe plating layer and tin were observed and analyzed by electron probe micro analyzer (EPMA) as shown Fig. 4-11. The Fe plating layer became thinner than the initial thickness (20ìm). Since the pure iron is oxidized very easily, it was regarded as the result by peeling of the Fe oxide layer. Intermetallic compounds of $FeSn_2$ were formed on the interface after peeling of the oxide layer.

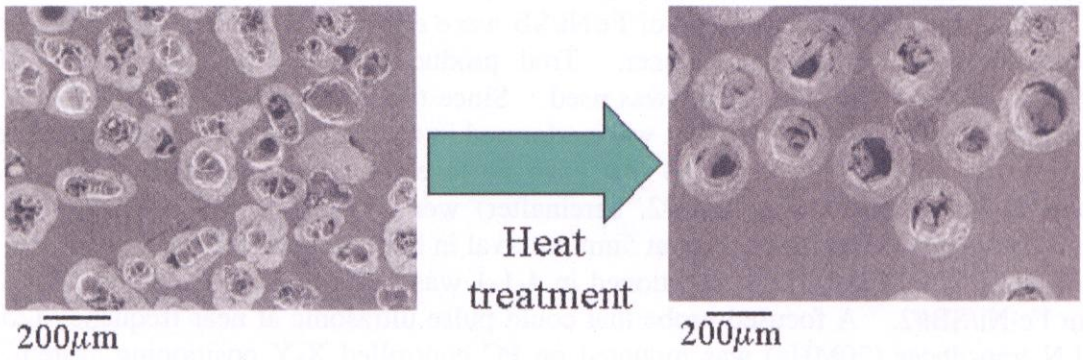

Fig. 4-9 Cross sectional view of Ni plated Sirasu balloons before and after heat treatment

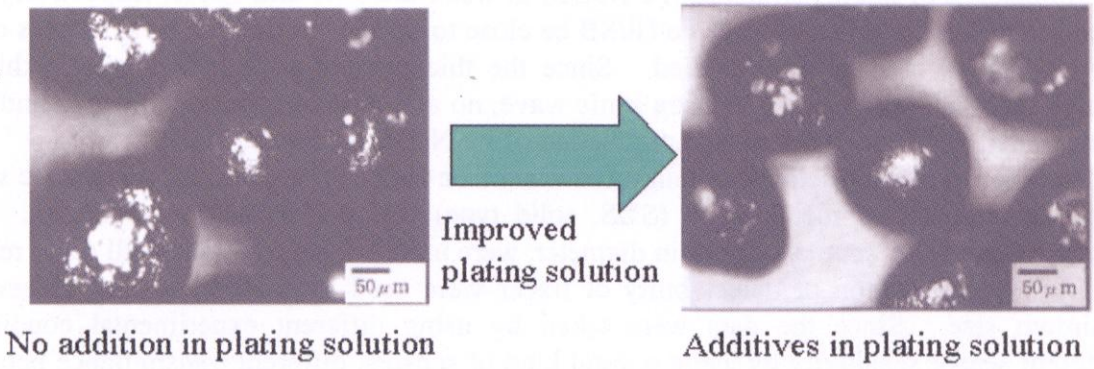

Fig. 4-10 Improved surface roughness of Ni plated Sirasu balloons

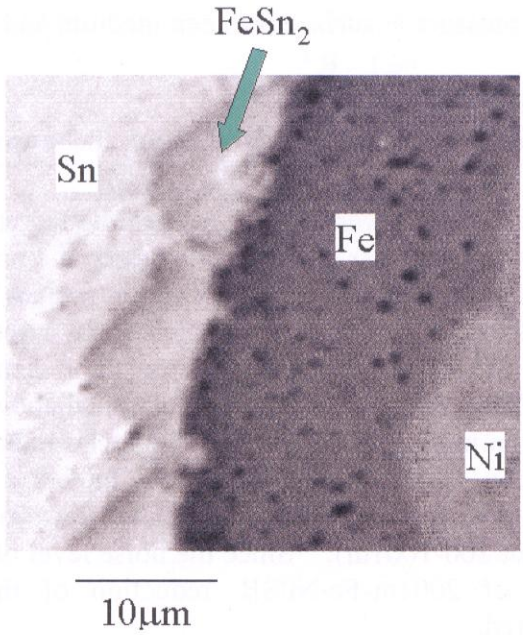

Fig. 4-11 Improved surface roughness of Ni plated Sirasu balloons

4.2.2 Acoustic Characteristics of Trial Production

Actual acoustic characteristics of Fe·Ni/SB were experimentally investigated in order to predict minimum diameter of tracer. Trial production of Fe·Ni/SB(Diameter:1000ìm, thickness of Fe: 10ìm and 20ìm) was used. Since the positioning of small balloon in the molten tin was difficult, experiment was performed in the water bath. Experimental setup is illustrated in Fig. 4-12. Fe·Ni/SB that have Fe layer of 10ìm in thickness (Fe·Ni/SB#1, hereinafter) and 20ìm (Fe·Ni/SB#2, hereinafter) were bonded at tip of needle-like rods. The rods were fixed on metal plate at 5mm interval in horizontal direction. The metal target (SUS, solid type) used in test mentioned in 4-1-1 was also fixed on same plate 5mm away from Fe·Ni/SB#2. A focused probe that could pulse ultrasonic at near frequency (25MHz) of LN transducer (20MHz) was mounted on PC controlled X-Y positioning system. The three targets were scanned at X-Y plane in water bath. One dimensional peak echo profiles and C-scope are shown in Fig. 4-13. The observed peak echo intensities of Fe·Ni/SB#1, #2 and metal target were almost equivalent. This result clearly suggests that reflectance of these three targets are almost equivalent. Actually, reflectance of steel (SUS target) in water and reflectance of bubble structure (Fe·Ni/SB) in water are 94% and 100%, respectively. It is expected that the reflectance of Fe·Ni/SB be close to 100%. Affection by thickness of Fe and Ni layers could be also studied. Since the thickness of the metal layers is thinner enough than half-wave length of ultra sonic wave, no affection of reflectance was found. It is concluded that reflectance of trial production of Fe·Ni/SB is close to 100%.

In order to predict detectable minimum size of Fe·Ni/SB in molten tin, parametric study changing diameter of metal target (SUS, solid type) was performed in molten tin. The targets, which were 2mm and 3mm in diameter, were used. This results and all other results obtained for evaluation of detectability of tracer were used in order to predict observable minimum size. Since the data were taken by using different experimental conditions (different sensor sensitivity by using several kind of sensors, different transmittance between sensor and glass or water or molten tin), all the data were converted by following formula for normalizing sensitivity of sensor and transmittance.

$$\text{Normalized echo intensity} = \frac{\text{echo intensity of target}}{A \cdot T} \quad (4\text{-}1),$$

A (sensor sensitivity) = echo level of sensor head

T (transmittance of sound pressure at surface between medium and sensor head)

$$= 1 - R^2 \quad (4\text{-}2),$$

R (Reflectance of sensor head)

$$= \frac{\text{echo level at surface between medium and sensor head}}{\text{echo level of sensor head}} \quad (4\text{-}3),$$

The normalized echo intensities were plotted against the target diameter as shown in Fig. 4-14. The solid line shows that linear correlation between the normalized echo intensity of SUS·solid type target (Diameter: 1mm, 2mm and 3mm) in molten tin and the target diameter. Since the gradient of this linear correlation is equivalent in all cases of targets, the broken line are expected in case of SUS·hollow type in molten tin. Hence, the echo intensity of SUS·solid type and Fe·Ni/SB were almost same as mentioned above. Therefore, dashed line can be plotted as correlation in case of Fe·Ni/SB. The echo intensities of glass·hollow type target lie on this correlation. This suggests that echo intensity of Fe·Ni/SB is essentially same as that of glass·hollow target, which was obtained last year (This means detectable minimum diameter is about 200-100ìm). Since the noise level of inside of sensor head was higher than echo level of 200ìm-Fe·Ni/SB, reduction of this noise level or signal conditioning will be required.

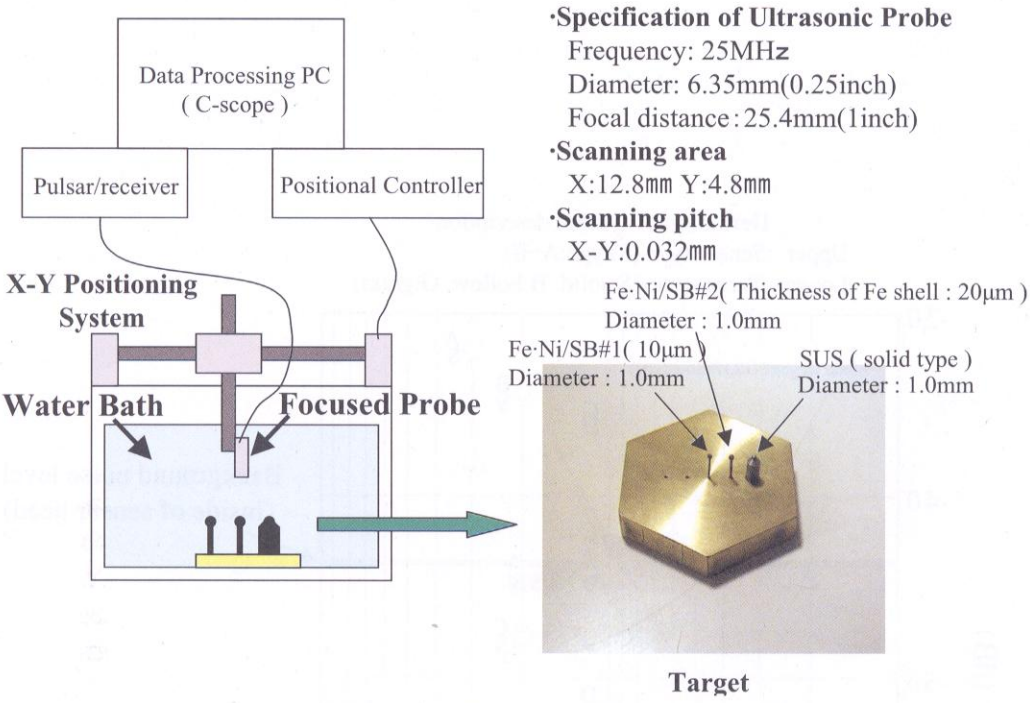

Fig. 4-12 Experimental set up for measuring detectability of tracer

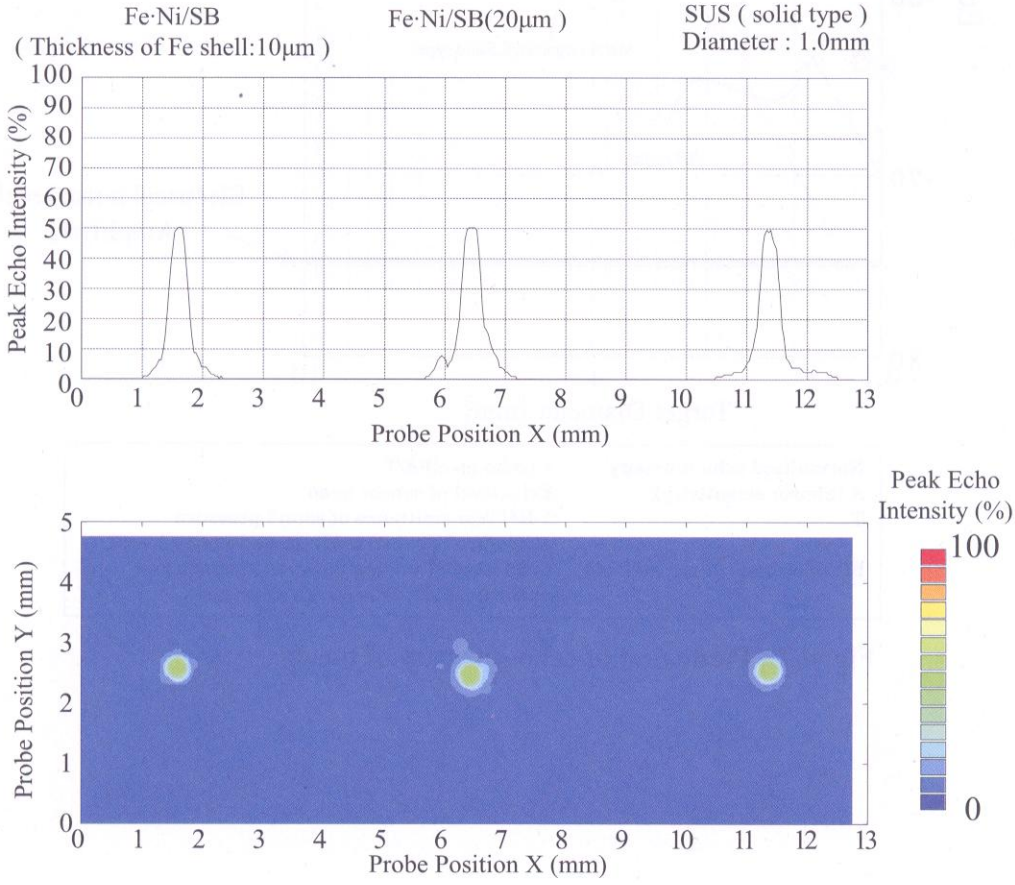

Fig. 4-13 Peak echo profile and C-scope of tracers

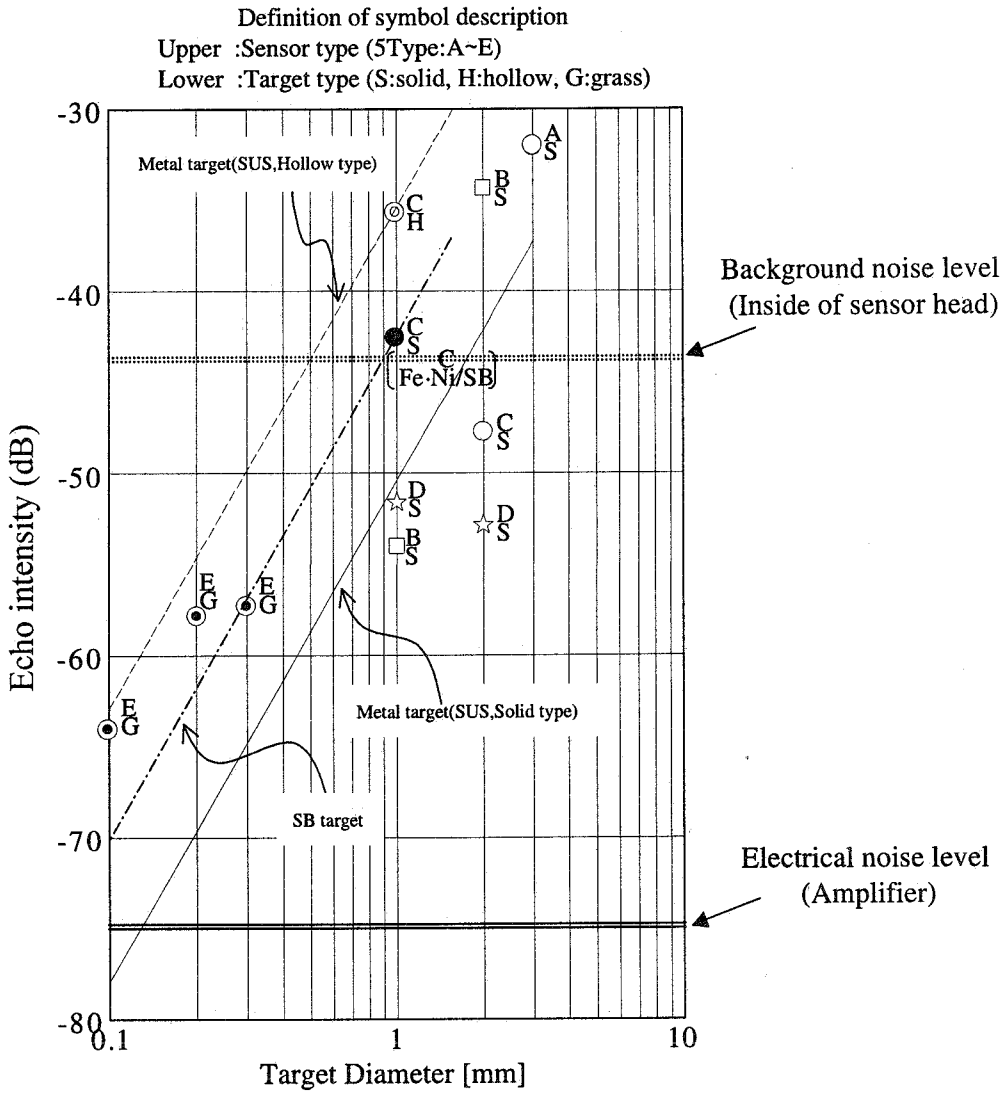

Normalized echo intensity	:= (echo level)/A/T
A (Sensor sensitivity)	:Echo level of sensor head
T	:1-R^2 (Transmittance of sound pressure at surface between medium and sensor head)
R(Reflectance of sensor head)	:Echo level of surface between medium and sensor head /Echo level of sensor head

Fig. 4-14 Prediction of echo intensity of tracer

5. COCLUSIONS

The following conclusions were obtained from the present studies.

(1) Measuring performances (measuring size, frequency characteristics, amplitude of temperature fluctuation) of radiation thermometer were experimentally verified. It was clarified that the performance was enough for measuring surface temperature fluctuation of oscillatory flow.

(2) These verifications mentioned above made an experimental result of thermocapillary flow with molten tin reliable and accurate. The first and clear experimental evidence for the transition from the steady flow to the oscillatory one was presented by the non-contact temperature measurement of a molten tin surface and the surface flow visualization. Imaishi *et al* confirmed validity of the experimentally determined Ma_{c2} and the frequency of the standing wave in comparison with a numerical result.

(3) The effect of an aspect ratio (As) of molten tin column on the Ma_{c2} was investigated by the temperature fluctuation measurement. When the As decreased, the Ma_{c2} increased monotonously. This tendency became remarkable especially when the As was less than 1.5. Internal temperature field of liquid bridge at the stable oscillatory flow was speculated by the phase relation analysis of the simultaneous multi-measurement data of surface temperature. The probable temperature fields were presented. The numerical simulation under the same conditions as the experiment was also conducted in order to inspect the onset point and temperature fluctuation data obtained by the experiment.

(4) The surface tension of molten tin was systematically measured at various temperatures between 523 and 1023K under the oxygen partial pressures (P_{O2}) between 10^{-19} and 10^{-6}MPa. The temperature coefficient of surface tension at a constant P_{O2} raised as P_{O2} increased and the sign of the coefficient changed from minus to plus at log P_{O2}= –9.375MPa. A thermocapillary experiment of molten tin is usually carried out at temperatures of 570-770K, and the estimated P_{O2} at the chamber outlet was in the order of 10^{-9}Pa (log P_{O2}= –15MPa). Therefore, it is concluded that an appropriate value of the surface tension coefficient for the present experiment chamber is -0.9×10^{-4}N/mK.

(5) Test for evaluating sensitivity of transducer at high temperature condition same as actual thermocapillary experiment was performed in molten tin. High spatial resolution was obtained in the direction of wave propagation. Numerical simulation was performed in order to check visualization performance of ongoing sensor-design. It was confirmed that tracers in molten tin liquid bridge could be visualized.

(6) The sphericity and surface roughness of Fe·Ni/SB were improved by a certain heat treatment technique on Ni plating process and by the organic additives to the Fe plating solution. The endurance of Fe·Ni/SB against molten tin was examined. It was confirmed that most of tracers were not collapsed but contained in tin melt after the experiment. Acoustic characteristics of Fe·Ni/SB were experimentally studied.

REFERENCES

[1] H. Kuhlmann, in: Hydrodynamic Instabilities in Thermocapillary Flows, Microgravity Science Technology VII/2 (1994) 75.

[2] N. Imaishi, S. Yasuhiro, T. Sato, and S. Yoda, in: Proc. 44th SPIE Annual Meeting and Exhibition, Materials Research in Low Gravity II, Denver, **3792** (1999) 344.

[3] N. Imaishi, S. Yasuhiro, and S. Yoda, in: Marangoni Convection Modeling Research Annual Report (NASDA-TMR-000006E), National Space Development Agency of Japan (2000) 157.

[4] S. Nakamura, T. Hibiya, K. Kakimoto, N. Imaishi, S. Nishizawa, A. Hirata, K. Mukai, S. Yoda, and T. Morita, J. Crystal Growth, **186** (1998) 85.

[5] T. Hibiya, S. Nakamura, N. Imaishi, K. Mukai, K. Onuma, P. Dold, A. Cröll, K-W. Benz, and S. Yoda, in: Proc. Joint 1st Pan-Pacific Basin Workshop and 4th Japan-China Workshop on Microgravity Sciences, Tokyo (1998) 8.

[6] J. Han, Z. Sun, L. Dai, J. Xie, and W. Hu, J. Crystal Growth, **169** (1996) 129.

[7] Y.K. Yang and S. Kou, J. Crystal Growth, **222** (2001) 135.

[8] R. Imai, K. Takagi, M. Ohtaka, F. Ohtsubo, H. Natsui, and S. Yoda, in: Marangoni Convection Modeling Research Annual Report (NASDA-TMR-990007E), National Space Development Agency of Japan (1999) 71.

[9] K. Takagi, M. Ohtaka, H. Natsui, T. Arai, and S. Yoda, in: Marangoni Convection Modeling Research Annual Report (NASDA-TMR-000006E), National Space Development Agency of Japan (2000) 115.

[10] K. Takagi, M. Otaka, H. Natsui, T. Arai, S. Yoda, Z. Yuan, K. Mukai, S. Yasuhiro, and N. Imaishi, J. Crystal Growth, submitted.

[11] M. Ohtaka, K. Takagi, H. Natsui, T. Arai, and S. Yoda, in: Proc. 2nd Pan-Pacific Basin Workshop on Microgravity Sciences, Pasadena (2001) IF-1159.

[12] K. Takagi, M. Otaka, H. Natsui, T. Arai, and S. Yoda, J. Jpn. Soc. Microgravity Appl. (in Japanese), **18** (2001) 11.

[13] N. Imaishi, S. Yasuhiro, Y. Akiyama and S. Yoda : Presented at 3rd Int. Workshop on Modeling Crystal Growth, Stony Brook N.Y. (2000).

[14] N.Imaishi, S.Yasuhiro and Y. Akiyama, J. Jpn. Soc. Microgravity Appl. (in Japanese), **18** (2001) 2.

[15] K. Mukai, Z. Yuan, K. Nogi, and T. Hibiya, ISIJ International, **40** (2000) Supplement, S148.

[16] Z. Yuan, K. Mukai, K. Takagi, and M. Ohtaka, J. Jpn. Inst. Metals (in Japanese), **65**, (2001) 21.

[17] A Passerone, E. Ricci, and R. Sangiorgi, J. Material Sci., **25** (1990) 4266.

[18] T. Suzuki and K. Ara, "The simulation of ultrasonic propagation in inhomogeneous liquid sodium for visual inspection", 14th International Conference on NDE in the Nuclear and Pressure Vessel Industries, Stockholm Sweden, 24-26 September 1996